AFRL-RX-WP-TP-2012-0368

PLASTIC FLOW AND MICROSTRUCTURE EVOLUTION DURING THERMOMECHANICAL PROCESSING OF A PM NICKEL-BASE SUPERALLOY (PREPRINT)

S.L. Semiatin
Metals Branch
Structural Materials Division

K.E. McClary
Wright State University

A.D. Rollett and C.G. Roberts
Carnegie Mellon University

E.J. Payton
Federal Institute for Materials Research and Testing

F. Zhang
CompuTherm, LLC

T.P. Gabb
NASA Glenn Research Center

July 2012
Interim

AIR FORCE RESEARCH LABORATORY
MATERIALS AND MANUFACTURING DIRECTORATE
WRIGHT-PATTERSON AIR FORCE BASE, OH 45433-7750
AIR FORCE MATERIEL COMMAND
UNITED STATES AIR FORCE

REPORT DOCUMENTATION PAGE

Form Approved
OMB No. 0704-0188

1. REPORT DATE *(DD-MM-YY)*	2. REPORT TYPE	3. DATES COVERED *(From - To)*
July 2012	Technical Paper	1 June 2012 – 1 July 2012

4. TITLE AND SUBTITLE

PLASTIC FLOW AND MICROSTRUCTURE EVOLUTION DURING THERMOMECHANICAL PROCESSING OF A PM NICKEL-BASE SUPERALLOY (PREPRINT)

5a. CONTRACT NUMBER
In-house

5b. GRANT NUMBER

5c. PROGRAM ELEMENT NUMBER
63112F

6. AUTHOR(S)

S.L. Semiatin (RXCM)
K.E. McClary (Wright State University)
A.D. Rollett and C.G. Roberts (Carnegie Mellon University)
E.J. Payton (Federal Institute for Materials Research and Testing)
F. Zhang (CompuTherm, LLC)
T.P. Gabb (NASA Glenn Research Center)

5d. PROJECT NUMBER
3946

5e. TASK NUMBER

5f. WORK UNIT NUMBER
LM106500

7. PERFORMING ORGANIZATION NAME(S) AND ADDRESS(ES)

Metals Branch
Structural Materials Division
Air Force Research Laboratory, Materials and Manufacturing Directorate
Wright-Patterson Air Force Base, OH 45433-7750
Air Force Materiel Command, United States Air Force

8. PERFORMING ORGANIZATION REPORT NUMBER
AFRL-RX-WP-TP-2012-0368

9. SPONSORING/MONITORING AGENCY NAME(S) AND ADDRESS(ES)

Air Force Research Laboratory
Materials and Manufacturing Directorate
Wright-Patterson Air Force Base, OH 45433-7750
Air Force Materiel Command
United States Air Force

10. SPONSORING/MONITORING AGENCY ACRONYM(S)
AFRL/RXCM

11. SPONSORING/MONITORING AGENCY REPORT NUMBER(S)
AFRL-RX-WP-TP-2012-0368

12. DISTRIBUTION/AVAILABILITY STATEMENT

Approved for public release; distribution unlimited. Preprint to be submitted to Metallurgical and Materials Transactions

13. SUPPLEMENTARY NOTES

The U.S. Government is joint author of this work and has the right to use, modify, reproduce, release, perform, display, or disclose the work. PA Case Number and clearance date: 88ABW-2012-2093, 5 April 2012. This document contains color.

14. ABSTRACT

Plastic flow and microstructure evolution during sub- and super- solvus forging and subsequent supersolvus heat treatment of the powder-metallurgy superalloy LSHR (low-solvus, high-refractory) were investigated to develop an understanding of methods that can be used to obtain a moderately-coarse gamma grain size under well-controlled conditions. To this end, isothermal, hot compression tests were conducted over broad ranges of temperature (1144 - 1450K, or 871 - 1177°C) and constant true strain rate (0.0005 - 10 s-1). At low temperatures, deformation was generally characterized by flow-softening and dynamic recrystallization that led to a decrease in grain size. At high subsolvus temperatures and low strain rates, steady-state flow or flow hardening were observed. These latter behaviors were ascribed to superplastic deformation and microstructure evolution characterized by a constant grain size or concomitant dynamic grain growth, respectively. During supersolvus heat treatment following subsolvus deformation, increases in grain size whose magnitude was a function of the prior deformation conditions were noted.

15. SUBJECT TERMS

superalloys, isothermal forging, supersolvus annealing, grain size

16. SECURITY CLASSIFICATION OF:			17. LIMITATION OF ABSTRACT:	NUMBER OF PAGES	19a. NAME OF RESPONSIBLE PERSON (Monitor)
a. REPORT	b. ABSTRACT	c. THIS PAGE			Donna Ballard
Unclassified	Unclassified	Unclassified	SAR	54	19b. TELEPHONE NUMBER *(Include Area Code)* N/A

Plastic Flow and Microstructure Evolution during Thermomechanical Processing of a PM Nickel-Base Superalloy

S.L. Semiatin, K. E. McClary[a], A.D. Rollett[b], C.G. Roberts[b],
E.J. Payton[c], F. Zhang[d], and T.P. Gabb[e]

Air Force Research Laboratory, Materials and Manufacturing Directorate,
AFRL/RXLM, Wright-Patterson Air Force Base, OH 45433-7817, USA
[a] Physics Department, Wright State University, Dayton, OH 45435, USA
[b] Materials Science & Engineering Department, Carnegie Mellon University,
Pittsburgh, PA 15213, USA
[c] Federal Institute for Materials Research and Testing, 12205 Berlin, Germany
[d] CompuTherm, LLC, Madison, WI 53710, USA
[e] NASA Glenn Research Center, Cleveland, OH 44135, USA

ABSTRACT

Plastic flow and microstructure evolution during sub- and super- solvus forging and subsequent supersolvus heat treatment of the powder-metallurgy superalloy LSHR (low-solvus, high-refractory) were investigated to develop an understanding of methods that can be used to obtain a moderately-coarse gamma grain size under well-controlled conditions. To this end, isothermal, hot compression tests were conducted over broad ranges of temperature (1144 - 1450K, or 871 - 1177°C) and constant true strain rate (0.0005 - 10 s^{-1}). At low temperatures, deformation was generally characterized by flow-softening and dynamic recrystallization that led to a decrease in grain size. At high subsolvus temperatures and low strain rates, steady-state flow or flow hardening were observed. These latter behaviors were ascribed to superplastic deformation and microstructure evolution characterized by a constant grain size or concomitant dynamic grain growth, respectively. During supersolvus heat treatment following subsolvus deformation, increases in grain size whose magnitude was a function of the prior deformation conditions were noted. A transition in flow behavior from superplastic to non-superplastic and the development during forging at a high subsolvus temperature of a wide (possibly bi- or multi- modal) gamma-grain-size distribution having some large

grains led to a substantially coarser grain size during supersolvus annealing in comparison to that produced under all other forging conditions.

Key words: Superalloys, isothermal forging, supersolvus annealing, grain size

I. INTRODUCTION

Nickel-base superalloys required for high-temperature applications in the aerospace and power-generation industries are frequently made by powder-metallurgy (PM) or directional solidification (DS) approaches [1]. The PM method is most common for rotating components that require high tensile and fatigue strength and a modicum of resistance to creep at temperatures of the order of 925K (652°C).

Pre-alloyed superalloy powders are usually made by spray atomization and are consolidated by hot isostatic pressing (HIP) or blind-die compaction followed by hot extrusion. PM billets so produced have a relatively fine gamma grain size (~5 microns) and a uniform distribution of second-phase precipitates such as gamma prime. At elevated processing temperatures, this microstructure yields low flow stress and high strain rate sensitivity typical of superplastic flow and is therefore useful in part fabrication via closed-die, isothermal forging. To improve the resistance to creep and creep-crack growth under dwell-fatigue loading in service, final heat treatment above the solvus temperature of the strengthening precipitates is often conducted to increase the gamma grain size to values of the order of 50 μm. Such finishing operations are usually applied uniformly to a component, but can also be applied locally for those regions of a component which experience the highest temperatures, thus forming the basis for dual-microstructure heat treatments [2-6].

A number of prior investigations have been conducted to establish the effect of thermomechanical processing variables on plastic flow and microstructure evolution in PM nickel-base superalloys. One of the earliest efforts was the comprehensive work of Immarigeon and Floyd for the PM superalloy 713LC [7]. They demonstrated the importance of initial grain size on subsolvus plastic flow. Three distinct behaviors depending on the initial grain size relative to the equilibrium grain size characteristic of superplastic flow were found. When the initial grain size was less than, equal to, or greater than the equilibrium value, flow-hardening, steady-state, or flow-softening behavior was observed, respectively. In turn, these three types of observations were ascribed to dynamic grain growth, classical superplastic flow under constant grain-size conditions, and dynamic recrystallization to a finer grain size. Furthermore, grain-size coarsening or refinement was shown to lead to transitions between so-called stage II (superplastic) flow largely characterized by grain/interphase boundary sliding and stage III (power-law creep) flow primarily due to the glide and climb of dislocations within the interior of grains.

The foundational work of Immarigeon and Floyd [7] was extended by a number of subsequent efforts [8-14]. For example, Combres and Levaillant [8] quantified the earlier observations and examined the broad influence of grain-size distribution on superplastic flow. Koul and Immarigeon [9] developed an isostress constitutive model to describe the plastic flow of initially coarse-grain materials as they recrystallize and become superplastic during isothermal forging. Using modern electron-backscatter-diffraction (EBSD) tools, Tu and Pollock [12-14] shed light on the strain-storage mechanisms postulated in early work in the area of superplasticity of PM superalloys.

Because two-phase alloys are often susceptible to the growth of abnormally large grains (several hundred microns in size or greater) during heat treatment [15], PM superalloy research has also focused on microstructure evolution during supersolvus heat treatment. For instance, Soucail, Huron, and their coworkers [16, 17] have shown that subsolvus isothermal forging at strain rates near the transition from stage II to stage III plastic flow are quite detrimental with regard to abnormal grain growth (AGG) during subsequent supersolvus heat treatment. It has been suggested as well that variables such as subsolvus exposure temperature, the heating rate to the solvus (and thus the rate at which pinning particles dissolve), and the location of pinning particles relative to larger or smaller grains in the grain-size distribution may also play an important role in the occurrence of AGG [18-21]. Based on these fundamental investigations, the efficacy of processing routes that impose limits on the strain rate during isothermal forging (to maintain superplastic conditions) and the control of carbon level (to ensure a minimum amount of various carbide phases which are stable above the solvus and can pin the gamma grain boundaries) on preventing AGG has been demonstrated [22-25]. The benefit of slightly higher temperatures and slightly lower strain rates during subsolvus isothermal forging (relative to typical practices) on preventing AGG but obtaining somewhat coarser gamma grain sizes during supersolvus heat treatment (which may improve creep-crack-growth resistance) has also been postulated [26].

The research reported here was part of a larger program to establish methods to produce controlled microstructure gradients in PM superalloys. The specific objective of the present work was to establish the effect of isothermal forging variables on plastic

flow behavior and grain growth during subsequent supersolvus heat treatment of an advanced PM superalloy.

II. MATERIALS AND PROCEDURES

A. *Materials*

The materials used in the present work were identical to those utilized in a previous investigation of the Smith-Zener pinning phenomenon [27]. They comprised three lots of the advanced gamma-gamma prime PM superalloy LSHR (denoting "low-solvus, high refractory"), developed by NASA for jet-engine disks. LSHR provides an attractive balance of properties at the bore and rim of disks subjected to a graded-microstructure heat treatment in which only the component rim is exposed above the solvus temperature to promote local growth of the gamma grains [28, 29]; the exposure time may vary from minutes to several hours [2-6]. The gamma-prime solvus, $T_{\gamma'}$, of this alloy is 1430K (1157°C).

The materials were received as (a) 170-mm-diameter, 40-mm-thick, isothermally-forged pancake, (b) 230-mm-diameter extruded billet, and (c) 75-mm-diameter billet which had been fabricated by further extrusion of the 230-mm-diameter billet. The materials had been produced by standard techniques starting with gas-atomized powder with a mesh size less than 325 (for the forged pancake) or 400 (for the extrusions); the average powder-particle sizes were approximately 32 and 27 μm, respectively. Following atomization, the powder for the pancake was subjected to a series of subsolvus operations comprising HIP consolidation, canned hot extrusion to a 5:1 reduction, and isothermal forging of a cylindrical preform to a 5:1 reduction. The powder for the billet products was also subsolvus HIP'ed followed by a single 6:1

reduction extrusion (230-mm-diameter billet) or a three-stage extrusion which included additional 2:1 and 4.5:1 reductions (75-mm-diameter billet). Although both the pancake and billet were final processed at similar subsolvus temperatures, the strain rates involved in such operations vary by approximately three orders of magnitude. Hence, the present R&D for such different materials served to determine the possible effect of preform condition on subsequent plastic flow and microstructure evolution.

The compositions of the pancake and extrusions were similar except for the levels of carbon and boron (Table I). The microstructure of the as-received materials comprised fine equiaxed grains whose average size was 2-2.5 μm in each material.

B. *Hot Compression Testing*

Isothermal, hot compression testing and supersolvus furnace heat treatment were used to evaluate plastic flow and microstructure evolution during thermomechanical processing (TMP) of the various lots of LSHR. For this purpose, cylindrical compression samples measuring 10-mm diameter x 15-mm height were machined from the pancake forging and slices of the two extrusions; test samples were extracted from both the outer diameter and inner diameter of the extrusions to assess the effect of location (and thus initial microstructural non-uniformity) on behavior.

Hot compression samples were first coated with glass for lubrication. Following lubrication, the sample and silicon-nitride compression tooling (which were mounted in a 250 kN servo-hydraulic test system) were induction heated using an iron-chromium-aluminum alloy susceptor to a test temperature of 1144, 1283, 1311, 1339, 1366, 1408, or 1450K (871, 1010, 1038, 1066, 1093, 1135, or 1177°C) in approximately 10 minutes. Following a soak at temperature for an additional 10 or 60 minutes, each sample was

then compressed to an average axial (height) strain of 0.7*. Constant true strain rates of 0.0005, 0.01, 0.1, 1, and 10 s^{-1} were used. Following compression, the sample was lowered automatically and forced-air cooled.

True stress-true strain curves were determined from average pressure (p_{av}) - axial strain (ε) plots derived from the compression load-stroke data which were reduced assuming uniform deformation and corrected for the test-machine compliance. The neglect of friction was estimated to lead to maximum errors in the flow stress of the order of 3 percent for the sample geometry and height reduction used in the present work [30]. Sample calculations of the effect of deformation heating on the flow response at strain rates of 0.1 s^{-1} or greater indicated that the qualitative flow hardening/softening response was unchanged by such corrections.

The strain-rate sensitivity of the flow stress (m value) was determined from the continuous flow curves at a strain of approximately 0.01 (i.e., a strain at which variations in microstructure with strain rate were quite small). Selected strain-rate jump tests were also performed at various temperatures to an axial height strain of 1.1 to evaluate the evolution of the strain-rate sensitivity with strain. Most of these tests comprised imposing alternating strain rates of 0.0005 and 0.001 at strain increments of ~0.1. A few jump tests were also performed at 1408 K (1135°C) with alternating strain rates of 0.005 and 0.01 s^{-1}.

C. *Microstructure Characterization*

Microstructure was evaluated in the as-compressed condition as well as after compression followed by supersolvus heat treatment. For the heat treatments, sections

* Compressive strains, strain rates, and stresses are reported as *positive* quantities here and throughout the balance of this work.

of compression samples were encapsulated in quartz tubes backfilled with argon and furnace heat treated for 1 h at 1444K (1171°C) followed by air cooling.

Following compression or compression + heat treatment, samples were sectioned axially. The sections were prepared using standard metallographic techniques, finishing by polishing with 0.05-μm colloidal silica. Grain structures were photographed using backscattered-electron (BSE) imaging in a scanning electron microscope (SEM) equipped with a field-emission gun (XL-30 or Quanta 600F, both manufactured by FEI, Hillsboro, OR). The grain structures in a number of samples were also analyzed via electron-backscatter diffraction (EBSD) in the XL-30 using EDAX/TSL OIM™ software (EDAX Corp., Mahwah, NJ). For this purpose, scans were performed over areas measuring approximately 10^4 to $5x10^6$ μm^2 using a step size between 0.5 and 5 μm; the specific parameters depended on the coarseness of the microstructure.

The average grain size and grain-size distribution (GSD) for each material and set of heat-treatment conditions were determined using the grain-delineation software in the EDAX/TSL OIM™ system and, in selected instances, via semi-automated image analysis using at least 5 BSE micrographs with FoveaPro™ (Reindeer Graphics, Asheville, NC) / Adobe PhotoShop® software; the grain boundaries determined by EBSD were defined using a 15° criterion. During such evaluations, twins were removed automatically by applying the twin-removal ($\Sigma 3$, $\Sigma 9$ boundary) capability in the OIM™ software or manually (FoveaPro™ approach). Grain size was taken as the diameter (D) of a circle with area equivalent to that observed in section, and was thus an underestimate of the true (three-dimensional) diameter.

For samples compressed at subsolvus temperatures, the primary gamma-prime particles possessed orientations that were different from those of the adjacent gamma grains and exhibited similar Z-contrast. Hence, the reported grain sizes for most of these samples are averages of both the gamma and gamma-prime phases. For selected as-subsolvus-compressed samples, however, the two microstructural features were segmented using one of two methods. The first technique was based on the differing chemical composition of the two phases as inferred from SEM scans in which both EBSD and energy-dispersive-spectroscopy (EDS) composition data were collected [31]. The segmented microstructures were also used to estimate grain-size *distributions* for the gamma phase alone. For this purpose, only the average gamma grain size was estimated from the segmented data because of the somewhat small extent of such images due to the slowness of coupled EBSD-EDS measurements. Much larger, un-segmented EBSD data sets were then truncated at the lower end (heavily populated with gamma-prime particles) to ensure that the average grain size of the remaining dataset was identical to the average gamma grain size estimated from the companion segmented images. The validity of the EBSD-EDS approach for microstructure segmentation was verified via an alternate SEM technique based on a special etching procedure [32] that enabled highlighting the gamma-prime phase, albeit without clear delineation of the gamma grain boundaries.

For samples that were supersolvus heat treated following hot compression, the gamma-prime precipitates were very fine because of the moderate final cooling rate. Their effect on grain-size analysis was eliminated automatically because of their

coherence with the matrix (EBSD) or manually via hand painting (FoveaPro™ approach).

EBSD data for selected samples were also used to estimate grain-boundary-misorientation distributions, pole figures, and various metrics of the stored work associated with geometrically-necessary dislocations.

III. RESULTS AND DISCUSSION

The primary results from this research consisted of the plastic-flow behavior (flow curves and rate sensitivity), microstructure observations, and quantitative analysis of the grain structures developed during TMP. Each of these aspects is summarized and discussed below.

A. *Plastic-Flow Behavior*

1. *Flow curves*

Constant true strain rate, true stress-true strain curves exhibited shapes analogous to observations from previous investigations of hot working of PM superalloys which had focused on somewhat narrower ranges of temperature and strain rate than used in the present work. For most combinations of temperature and strain rate, the results for the isothermally forged pancake (Figure 1) were similar to those for the 230-mm-diameter extruded billet (Figure 2) and the 75-mm-diameter extruded billet (not shown). In particular, the stress-strain curves exhibited a range of behaviors characterized by moderate to extensive flow softening, steady-state flow, or moderate-to-strong flow hardening (Figures 1 and 2, Table II).

For compression tests at temperatures below the gamma-prime solvus (i.e., T < 1430K (1157°C)), for example, the flow response for strain rates of 0.01 s^{-1} or greater

comprised an initial strain-hardening regime at low strains, a peak stress (sometimes associated with a short-yield point phenomenon), and then moderate-to-noticeable flow softening. Such flow curves are typical of materials undergoing discontinuous dynamic recrystallization (DDRX). For subsolvus tests at 0.0005 s^{-1} (Figure 3), the behavior was more complex. At T = 1283 K (1010°C), the peak-stress/flow-softening shape of the stress-strain curve (Figure 3b) was similar to that observed at higher strain rates. At the typical temperature used for isothermal forging of LSHR, viz., T = 1339 K (1066°C), on the other hand, the flow curve exhibited mild flow hardening (Figure 3a) or steady-state flow (Figure 3b). These behaviors are indicative of superplastic flow with somewhat limited or no dynamic grain growth. For the highest subsolvus temperature, 1408 K (1135°C), very noticeable flow hardening was observed in all three lots of LSHR tested at 0.0005 s^{-1}. As will be discussed in subsequent sections, this response was indicative of noticeable dynamic grain growth and a gradual transition from highly superplastic to somewhat less superplastic flow.

The flow behavior of samples tested above the solvus, i.e., at 1450 K (1177°C) was confounded by the occurrence of gross failure (strain rates of 1 and 10 s^{-1}) or extensive wedge cracking (strain rate ≤ 0.1 s^{-1}). Such defects were associated with the coarse grain size developed during preheating due to complete dissolution of the gamma-prime phase. Hence, the flow curves from experiments at the higher strain rates in Figures 1c, 2c are somewhat approximate and not indicative of actual material behaviors. The flow curves determined at the supersolvus temperature and a strain rate of 0.0005 s^{-1} (Figure 3) exhibited either steady-state flow or marked flow softening. The

rate-sensitivity measurements to be presented in the next section suggested that these behaviors were due to dislocation glide-climb processes.

Flow curve measurements were also useful in elucidating the effect of preheat time and billet location on plastic flow. For example, results for test temperatures of 1339 K (1066°C) and 1408 K (1135°C) (Figure 4a) showed higher flow stresses after a 60-minute preheat than a 10-minute preheat. This behavior was qualitatively similar for a strain rate of 0.0005 s^{-1} (i.e, in the superplastic flow regime) as well as for 0.01 s^{-1}, which lay in the transition range from superplastic to non-superplastic behavior. Such differences can result from static coarsening of the gamma-prime pinning particles and concomitant gamma grain growth during preheating; this effect is discussed further in Section III.B.

Experiments on samples taken from the outer and inner diameters (OD, ID) of the 230-mm-diameter billet revealed similar flow stresses for strain rates of 0.1 s^{-1} or greater. At 0.0005 and 0.01 s^{-1}, however, there were measurable differences in flow stress at the typical isothermal forging temperature (1339 K, or 1066°C) as well as at 1283 K (1010°C) (Figures 4b, c). These differences were ascribed to somewhat finer initial grain size at the OD location. Such a variation would most likely have arisen from different instantaneous processing temperatures that result from the competition between die-chilling and deformation heating during extrusion. The net effect of chilling and deformation heating on plastic flow would vary with radial location within the billet. Assuming a grain-size exponent of the flow stress of 2 for superplastic conditions [14], a variation in flow stress of ~30 pct., such as was observed at 1339 K (1066°C) / 0.0005 s^{-1}, would result from a grain size variation of only ~15 pct. The similarity in OD and ID

flow behaviors at 0.0005 and 0.01 s^{-1} and a test temperature of 1408 K (1135°C), which was above the nominal extrusion temperature, was most likely associated with microstructural changes during preheating which affected subsequent plastic flow.

2. *Strain-rate sensitivity of the flow stress*

Strain-rate-sensitivity (m value) measurements (Figure 5, Table III) supported the conclusions from the stress-strain curves regarding the mechanisms of plastic flow of the LSHR PM material. By and large, the trends were similar for the forged pancake, 230-mm-diameter billet, and 75-mm-diameter billet. For example, the data determined at small strain (~0.01) from the continuous flow curves for test temperatures of 1339 K (1066°C) and 1408 K (1135°C) exhibited the expected transition from high m values indicative of superplastic flow (~0.60) at strain rates of ~0.0005 – 0.01 s^{-1} to intermediate m values at strain rates of 0.01 – 0.1 s^{-1} and low m values indicative of power-law creep (~0.15 – 0.25) at higher strain rates (Figure 5). The corresponding data for the supersolvus test temperature 1450 K (1177°C) (Figure 5a) indicated a rate sensitivity of the order of ~0.26 over most of the strain-rate range, thus suggesting the occurrence of power-law creep due to the glide and climb of dislocations throughout the coarsened grain structure.

Data from the jump tests in which the strain rate was varied in an alternating fashion between 0.0005 and 0.001 s^{-1} provided additional insight into the evolution of m values and hence the deformation mechanism during large plastic flow (Table III). Results for strains of 0.15 and 0.85 at the lowest test temperature (1144 K, or 871°C) showed a small increase in m from ~0.15 to ~0.25; these values are nevertheless still indicative of power-law-creep behavior during the entire deformation. By contrast, the m

values for test temperatures of 1283 K (1010°C) and 1339 K (1066°C) were much higher (~0.6 – 0.7), typical of superplastic flow, and showed little variation with strain. The results for 1408 K (1135°C) (Table III) showed a third variation with strain, which was similar for all three lots of LSHR. In particular, the m values were relatively high at low strains (i.e., ~0.60 – 0.65), but decreased to lower values (~0.45 – 0.50) at higher strains. This trend suggested a gradual loss of superplastic behavior associated with the observed marked flow hardening (Figure 3) and, as will be shown in Section III.B, dynamic grain growth.

Selected subsolvus jump tests over the same strain-rate range, but following a *60-minute* preheat, indicated that static grain growth prior to deformation could have an effect on the m value similar to dynamic grain growth. For the longer-preheat-time experiments, the m values showed little dependence on strain and were ~0.6 – 0.7 at 1339 K (1066°C) and ~0.4 – 0.5 at 1408 K (1135°C). Similarly, the m values from jump tests conducted at 1408 K (1135°C) using alternating strain rates of 0.005 and 0.01 s^{-1} showed little variation with strain being approximately 0.40 for both lots of LSHR.

The m values for the supersolvus jump tests at 1450 K (1177°C) (Table III) also showed a decrease with increasing strain, but the specific trend varied with test material. For the forged pancake, the rate sensitivity decreased slightly from 0.3 to 0.23, or values well within the power-law-creep regime. The initial strain-hardening period followed by steady-state flow exhibited by the corresponding constant-strain-rate flow curve (Figure 3a) suggested the occurrence of plastic flow controlled by dynamic recovery. The m values for the 230-mm-diameter billet showed a decrease with strain of similar magnitude, but the specific values were somewhat higher (~0.35 – 0.40), thus

indicating a behavior that lay in the transition range between superplastic and power-law creep. However, the corresponding constant-strain-rate flow curve (Figure 3b) suggested the occurrence of dynamic recrystallization and thus the importance of the generation and annihilation of large numbers of dislocations.

B. *Microstructure Evolution*

1. *As-deformed microstructures*

Microstructure observations for the LSHR pancake and extruded billet materials were similar. The as-deformed microstructures were interpreted in the context of observations of samples that were given the same preheat and then water quenched (e.g., Figure 6 for LSHR pancake samples). Not surprisingly, these observations revealed a gradual increase in un-deformed grain size with increasing temperature. The most noticeable increase occurred above 1339 K (1066C), at which the volume fraction of the principal pinning phase below the solvus, i.e., the gamma-prime precipitates, decreased rapidly with increasing temperature. Compared to the as-preheated conditions, the microstructures for LSHR pancake samples deformed at 0.0005 s^{-1} (Figure 7) revealed a noticeable reduction in grain size at 1144 K (871°C), comparable grain size at 1339 K (1066°C), and a noticeable increase in grain size at 1408 K (1135°C). The limited or large degree of dynamic grain growth for experiments at 1339 K (1066°C) and 1408 K (1135°C), respectively, is further illustrated with the direct comparisons in Figure 8. Furthermore, the occurrence of static grain growth at 1408 K (1135°C) was ascertained by comparison of the microstructures preheated 10 or 60 minutes (Figures 8c, e). Additional grain-size observations and measurements for the LSHR pancake and extruded billet materials are summarized in Figure 9 and Table IV.

Below the solvus, the results in Table IV illustrate a general increase in grain size with increasing temperature and decreasing strain rate, as expected.

The as-deformed microstructure observations (Figures 7-9 and Table IV) corroborated conclusions regarding the mechanisms of subsolvus deformation drawn from the flow curves (Figures 1-3, Table II). For example, flow softening observations at all strain rates for T = 1144 K (871°C) and T = 1283 K (1010°C) (Table II) were indeed related to a reduction in grain size due to dynamic recrystallization (Table IV). At 1339 K (1066°C), near-steady state flow at 0.0005 s^{-1} (Table II) was related to an essentially constant grain size (Table IV), and flow softening at higher strain rates (Table II) was a result of dynamic recrystallization as evidenced by a reduction in grain size (Table IV). At 1408 K (1135°C), the transition from flow hardening response at 0.0005 s^{-1} to near-steady-state flow at 0.01 s^{-1} and then flow softening at higher strain rates was accompanied by dynamic grain growth, a limited change in grain size, or a grain-size reduction, respectively (Table IV). In addition, the effect of increasing preheat time on the initial flow stress [especially noticeable at 1408 K (1135°C), 0.0005 s^{-1} (Figure 4a)] can be rationalized on the basis of the observed static coarsening (Figures 8c, e).

Interpretation of the relation between the as-deformed microstructure and flow curves for deformation above the solvus (i.e., at 1450 K, or 1177°C; Figures 1c, 2c) was less clear, partly as a result of the occurrence of wedge cracking (Figure 7d). However, the appearance of partially-recrystallized microstructures appeared to be consistent with stress-strain behaviors that were a mixture of steady-state flow and flow softening (Table II).

The as-deformed microstructures also revealed a range of ratios “as-large-as” (ALA) grain size to average grain size (Table IV). Many of the values were between 3 and 5. However, some of the ratios, especially those for low temperature/high strain rate conditions, were higher, suggesting perhaps that recrystallization had not been completed or that some remnant large grains were present in the starting material.

2. *Compressed-and-supersolvus-heat-treated microstructure*s

A range of microstructures was produced during supersolvus heat treatment at 1444 K (1171°C) for 1 h following hot compression. Typical examples are shown in Figures 10 and 11; the corresponding grain size results are summarized in Table IV.

For deformation temperatures of 1339 K (1066°C) or lower and all strain rates (Figures 10a, b; Figures 11a, b, c), relatively uniform grain structures were developed during the supersolvus heat treatment. The average gamma grain size in these cases was ~15 -20 μm, and the ALA: average-grain-size ratios were generally in the range of 2 to 5 (Table IV). By way of comparison, as-received samples from the same lots of LSHR as used in the present work developed pinned grain sizes of ~15-20 μm and the ALA:average ratios were between ~2.5 and 3.5 during a similar supersolvus furnace heat treatment (1455 K, or 1182°C, for 2 h) [27].

The supersolvus heat treatment response of samples pre-deformed just below the solvus (i.e., at 1408 K, or 1135°C) or above the solvus (at 1450 K, or 1177°C) (Figures 10c, d; Figures 11d, e; Table IV) was dramatically different than that for samples deformed at lower temperatures. Specifically, the grain sizes were much larger. For subsolvus forging at 1408 K (1135°C), for example, the effect was particularly noticeable in the LSHR pancake material deformed at 0.0005 s^{-1} and in the

230-mm-diameter LSHR billet deformed at 0.01 s^{-1}. These conditions were those for which the m value decreased noticeably with strain (from ~0.60 to 0.45) or was ~0.40 over the entire strain range, respectively. Alternate heat-treatment times of 0.25 or 2 h at 1444 K (1171°C) did not materially affect these grain-size trends (Table V), except for the appearance of some scatter in the average grain size for 230-mm-diameter billet samples that had been pre-deformed at 1408 K (1135°C)/0.0005 s^{-1}.

The unusual microstructures developed during supersolvus heat treatment following supersolvus deformation appeared to be only partially recrystallized. Such observations were rationalized on the basis EBSD measurements which revealed that samples processed solely above the supersolvus (both as-compressed as well as compressed-and-heat-treated) contained a high fraction (~1/3) of low-mobility, low-angle boundaries.

3. *EBSD analysis of unusual grain-growth phenomenon*

Insight into the source of the unusual behavior for samples pre-deformed at 1408 K (1135°C) and then supersolvus heat treated was obtained from analysis of EBSD data. For this purpose, attention was focused on the as-deformed condition of pancake and 230-mm-diameter billet OD samples which had been preheated 10 minutes and then compressed using a strain rate of 0.0005 s^{-1} to a 2:1 reduction at either 1339 K (1066°C), the typical isothermal forging temperature, or 1408 K (1135°C), the higher-than-usual forging temperature which produced a much coarser average gamma grain size. Factors that were examined included the nature of stored work, crystallographic texture, grain-boundary-misorientation distribution, and the grain-size distribution per se.

The nature of the stored work was similar for both the pancake and extruded billet samples, and thus, for the sake of brevity, only results for the former lot of material are reported. In particular, EBSD-derived microstructures indicating the high- and low-angle grain boundaries showed that material deformed at 1408 K (1135°C) did exhibit more grains with internal subgrains than samples deformed at 1339 K (1066°C) (Figure 12). However, most of the grains, even in the higher temperature samples, contained no sub-boundaries at all. Furthermore, measurements of grain average misorientation (GAM), grain-reference-orientation deviation (GROD), and grain-orientation spread (GOS) were similar for samples deformed at the two temperatures (Figure 13). These indices, which quantify the distortion of the crystal lattice due to the retention of geometrically-necessary dislocations, were also relatively small in magnitude.

The crystallographic textures and the character of the grain-boundary misorientations of the samples deformed at 1339 K (1066°C) and 1408 K (1135°C) were also similar (Figure 14) and consistent with superplastic (or near-superplastic deformation). For example, the as-deformed textures were all relatively weak with a maximum intensity of ~2 x random (Figures 14a, b). The grain-boundary misorientaion distributions were almost random in every case as well, as indicated by their similarity to the Mackenzie distribution [33] (Figures 14c, d).

A comparison of the grain-size distribution (GSD) of samples deformed at the two different temperatures to a 2:1 reduction at 0.0005 s^{-1} did show some subtle differences (Figure 15). For instance, the GSD of LSHR pancake samples deformed at 1339 K (1066°C) exhibited what appeared to be log-normal-like behavior (Figure 15a). This observation was supported somewhat by the corresponding probability plot of the

normalized grain size (Figure 15c), which showed nearly linear behavior except for the not unusual tail at the low end of the distribution. Such a tail was associated with the large number of finer particles of primary gamma-prime each of whose orientations was dissimilar from the gamma grains but which could not be differentiated by standard EBSD techniques due to the similarity in crystal structure of the two phases. The GSD for LSHR pancake samples compressed at 1408 K (1135°C) revealed a slightly less log-normal trend as indicated by the somewhat high frequency of grains with intermediate grain sizes (Figure 15b) and slightly sigmoidal shape of the corresponding probability plot (Figure 15d).

A clearer picture of pertinent microstructural features in as-compressed samples was obtained from results in which the gamma and gamma-prime phases were segmented based on composition differences; i.e., EBSD/EDS scans. Examples of such results for the LSHR pancake and the 230-mm-diameter LSHR billet deformed at either 1339 K (1066°C) or 1408 K (1135°C) (Figure 16) revealed gamma grains (colored phase) which were considerably larger than the primary gamma-prime particles (black phase). The average diameter of the gamma-prime particles for each of the four samples was ~1.8 μm. The volume fraction of gamma prime at 1339 K (1066°C) was approximately 0.175 for both materials. At 1408 K (1135°C), the measured difference in gamma-prime volume fraction (viz., 0.045 for the pancake material and 0.09 for the billet material) may be due to slight variations in composition (Table I) and the very sharp gradient in the gamma-prime approach curve near the solvus temperature.

An examination of the location of the gamma-prime particles in the segmented as-compressed microstructures (Figure 16) showed some important differences among

the various samples. For samples of both the pancake and billet materials compressed at 1339 K (1066°C), the gamma-prime particles lay primarily at the gamma grain boundaries (Figures 16a, c). A similar trend was seen for the billet sample deformed at 1408 K (1135°C) (Figure 16d). By contrast, a large number of gamma-prime particles lay *within* gamma grains for the pancake sample deformed at 1408 K (1135°C) (Figure 16b). The presence of interior gamma-prime particles was especially obvious for the larger gamma grains. A number of these larger gamma grains also tended to have unusual shapes, reminiscent of abnormal grains often seen in the literature [15], and sharp radii of curvature which would provide a high driving force for local boundary migration. The present observations are also similar to the findings of Dennis, et al. [34] who noted that the boundaries of abnormally growing grains in Al-3.5Cu had a lower fraction of pinning particles per unit area. Furthermore, the observed variation in the location of primary gamma-prime particles immediately following subsolvus deformation may play an important role in the tendency for subsequent supersolvus grain growth which is abnormal (or nearly abnormal), as has been postulated in theories which focus on non-uniform grain unpinning due to the dissolution of second phase particles [19-21].

Approximate GSD data for the gamma phase alone, determined from the segmented images per the approach outlined in Section II.C, were sorted using two different bin sizes. Results for the as-compressed LSHR pancake and 230-mm-diameter billet samples (Figures 17 and 18, respectively) revealed a noticeable dependence on deformation temperature. For both materials, the as-compressed gamma-grain GSDs for samples compressed at 1339 K (1066°C)/0.0005 s^{-1} showed relatively smooth, log-normal-like shapes (Figures 17a, b and Figures 18a, b). On the

other hand, samples compressed at 1408 K (1135°C)/0.0005 s^{-1} revealed bi- or multi-modal shape in the corresponding GSDs (Figures 17c, d and Figures 18c, d). The degree of irregularity was noticeably greater for the LSHR pancake material. These differences were also observed somewhat in the corresponding probability plots of the normalized grain sizes (not shown).

The gamma-grain GSDs in Figures 17 and 18 exhibited two additional characteristics that may have affected subsequent supersolvus grain-growth response. First, the absolute width of the distributions (in microns) was much narrower for pancake and 230-mm diameter samples deformed at 1339 K (1066°C)/0.0005 s^{-1} (Figures 17a, b and 18a, b) compared to those for samples deformed at 1408 K (1135°C)/0.0005 s^{-1} (Figures 17c, d and 18c, d). Second, the higher-deformation-temperature GSDs (in particular that for the pancake material) revealed that some of the grains had a size greater than the stable-pinned (Smith-Zener) grain size of 15-20 μm. As the simulation work of Wang, et al. [21] has suggested, a wide GSD containing some grains whose size exceeds the Smith-Zener limit may be particularly susceptible to abnormal grain growth as the pinning particles dissolve. The present experimental grain-size results for samples given a supersolvus heat treatment following hot compression (Tables IV and V) did indeed show that LSHR pancake material pre-deformed at1408 K (1135°C)/0.0005 s^{-1} exhibited a final average grain size and ALA size substantially larger than most of the other samples. Such behavior may thus be concluded to be at least partially related to the nature of the gamma GSD and gamma-prime particle location developed during isothermal forging.

IV. SUMMARY AND CONCLUSIONS

Isothermally-forged pancake and extruded billet of the PM superalloy LSHR were subjected to isothermal hot compression and final supersolvus heat treatment in order to establish the effect of TMP sequence on plastic flow and microstructure evolution. The following conclusions were drawn from this work:

1. Plastic flow during constant-strain-rate, isothermal hot compression is characterized by one of three behaviors depending on strain rate and temperature. At low temperatures and high strain rates, flow softening due to discontinuous dynamic recrystallization is observed. At higher subsolvus temperatures and low strain rates, steady state flow indicative of grain/interphase boundary sliding and limited grain growth occurs. At temperatures just below the solvus and low strain rate, flow hardening associated with dynamic grain growth occurs.

2. Static grain growth below the solvus due to extended soak time prior to deformation can lead to higher initial flow stresses compared to the behavior for short time preheating of PM superalloys.

3. Static and dynamic grain growth can both lead to the loss of superplastic properties during hot deformation, especially during processing below the solvus temperature. Such loss of superplasticity is characterized by a decrease in m values from $\geq$0.6 to ~0.45 with increasing strain (dynamic grain growth) or low/constant m values of the order of 0.4-0.45 (static grain growth prior to deformation).

4. The loss of superplastic properties such as occurs as a result of dynamic grain growth during slow rate deformation below the solvus can yield substantially coarser gamma grain sizes (while avoiding grossly abnormal grain growth) during subsequent

supersolvus heat treatment compared to that developed using typical isothermal (slow strain rate) or conventional (high strain rate) hot forging practices prior to supersolvus heat treatment. Such “hot, slow” approaches appear to depend on the development of an as-forged microstructure characterized by (1) a wide gamma grain-size distribution (which may be bi- or multi-modal) with some grains larger than the nominal Smith-Zener limit and (2) a reduction in the grain boundary area pinned by gamma-prime particles, especially for larger grains. These two factors may lead to the non-uniform elimination of the pinning force and preferential growth of larger gamma grains upon heating above the solvus temperature.

Acknowledgements – This work was conducted as part of the in-house research of the Metals Branch of the Air Force Research Laboratory’s Materials and Manufacturing Directorate. The support and encouragement of the Laboratory management are gratefully acknowledged. The assistance of P.N. Fagin and T.M. Brown in conducting the experiments and A. Shively, A.L. Pilchak, and A.A. Salem in segmenting EBSD/EDS data is greatly appreciated. Technical discussions with P.L. Martin (AFRL) and J. Gayda and J. Telesman (NASA GRC) are also much appreciated. Two of the authors (ADR and CGR) also acknowledge support from the Air Force STW-21 Initiative, Contract F33615-01-2-5225, and the MRSEC at Carnegie Mellon University, NSF Grant Number DMR-0520425.

REFERENCES

1. M.J. Donachie Jr, ed., *Superalloys Source Book*, ASM International, Materials park, OH, 1984.
2. J. Gayda, T.P. Gabb, and P.T. Kantzos: US Patent 6,660,110, December 2003.
3. S.L. Semiatin and D.R. Barker: US Patent 5,447,580, September 1995.
4. G.F. Mathey: US Patent 5,312,497, May 1994.
5. S. Ganesh and R.G. Tolbert: US Patent 5,527,020, June 1996
6. J. Lemsky: Unpublished research, Ladish Co., Cudahy, WI, 2006.
7. J-P.A. Immarigeon and P.H. Floyd: *Metall. Trans. A*, 1981, vol. 12A, pp. 1177-1186.

8. A.K. Koul and J-P.A. Immarigeon: *Acta Metall.*, 1987, vol. 35, pp. 1791-1805.

9. Y. Combres and C. Levaillant: *Inter. J. Plasticity*, 1990, vol. 6, pp. 505-519.

10. M.O. Alniak and F. Bedir: *Mater. Sci. Eng. A*, 2006, vol. A429, pp. 295-303.

11. M.O. Alniak and F. Bedir: *Mater. Sci. Eng. B*, 2006, vol. B130, pp. 254-263.

12. W. Tu and T.M. Pollock: *Superalloys 2008*, R.C. Reed, K.A. Green, P. Caron, T.P. Gabb, M.G. Fahrmann, E.S. Huron, and S. A. Woodard, eds. TMS, Warrendale, PA, 2008, pp. 395-403.

13. W.J Tu: PhD Dissertation, University of Michigan, Ann Arbor, MI, 2010.

14. W.J. Tu and T.M. Pollock: *Metall. Mater. Trans. A*, 2010, vol. 41A, pp. 2002-2009.

15. J.W. Martin, R.D. Doherty, and B. Cantor: *Stability of Microstructure in Metallic Systems*, Cambridge University Press, Cambridge, UK, 1997.

16. M. Soucail, M. Marty, and H. Ocor: R.D. Kissinger, D.J. Deye, D.L. Anton, A.D. Cetel, M.V. Nathal, T.M. Pollock, and D.A. Woodford, eds., TMS, Warrendale, PA,1996, pp. 663-666.

17. E. Huron, S. Shrivatsa, and E. Raymond: *Superalloys 2000*, T.M. Pollock, R.D. Kissinger, R.R. Bowman, K.A. Green, M. McLean, S. Olson, and J.J. Schirra, eds., TMS, Warrendale, PA, 2000, pp. 49-58.

18. E.J. Payton: PhD Dissertation, The Ohio State University, Columbus, OH, 2009.

19. P.R. Rios: *Acta Mater.*, 1997, vol. 45, pp. 1785-1789.

20. K. Song and M. Aindow: *Proc. Materials Science and Technology (MS&T) 2006: Fundamentals and Characterization, Vol. 2*, Z-K. Lu, C.E. Campbell, L.Q. Chen, E. B. Damm, J.E. Morral, and J.L. Murray, eds., TMS, Warrendale, PA, 2006, pp. 211-220.

21. G. Wang, D.S. Xu, E.J. Payton, N. Ma, R. Yang, M.J. Mills, and Y. Wang: *Acta Mater.*, 2011, vol. 59, pp. 4587-4594.

22. T.P. Gabb, J. Gayda, and J. Falsey: Report NASA/TM-2005-213649, National Aeronautics and Space Administration, Glenn Research Center, Cleveland, OH, June 2005. (Available electronically at http://gltrs.grc.nasa.gov)

23. D.D. Krueger, R.D. Kissinger, R.G. Menzies, and C.S. Wukusick: US Patent 4,957,567, September 1990.

24. E.L. Raymond, R.D. Kissinger, A.J. Paxson, and E.S. Huron: US Patent 5,584,947, December 1996.

25. E.S. Huron, J.A. Heaney, D.P. Mourer, J.R. Groh, E.L. Raymond, D.A. Utah, M.J. Weimer, and K.R. Bain: US Patent Application 11/770,257, January 2009.

26. D.P. Mourer and K.R. Bain: US Patent Application 12/494,896, December 2010.

27. S.L. Semiatin, K. E. McClary, A.D. Rollett, C.G. Roberts, E.J. Payton, F. Zhang, and T.P. Gabb: *Metall. Mater. Trans. A*, 2012, vol. 43A, in press.

28. J. Gayda, T.P. Gabb, and P.T. Kantzos: *Superalloys 2004*, K.A. Green, T.M. Pollock, H. Harada, T.E. Howson, R.C. Reed, J.J. Schirra, and S. Walston, eds. TMS, Warrendale, PA, 2004, pp. 323-330.

29. J. Lemsky: Report NASA/CR-2005-213574, Ladish Company, Inc., Cudahy, WI, February 2005. (Available electronically at http://gltrs.grc.nasa.gov)

30. S.I. Oh, S.L. Semiatin, and J.J. Jonas: *Metall. Trans. A*, 1992, vol. 23A, pp. 963-975.

31. A.A. Salem, M.G. Glavicic, and S.L. Semiatin: *Mater. Sci. Eng. A*, 2008, vol. A494, pp. 350-359.

32. E.J. Payton, P.J. Phillips, and M.J. Mills: *Mater. Sci. Eng. A*, 2010, vol. A527, pp. 2684-2692.

33. J.K. Mackenzie: *Biometrika*, 1958, vol. 45, pp. 229-240.

34. J. Dennis, P.S. Bate, and F.J. Humphreys: *Acta Mater.*, 2009, vol. 57, pp. 4539-4547.

Table I. Chemical Composition (Weight Pct.) of LSHR Program Materials

Material	Co	Cr	Al	Ti	Mo	W	Nb	Ta	C	B	Zr	Ni
Pancake	20.5	12.4	3.6	3.5	2.8	4.3	1.5	1.2	0.03	0.02	0.05	Bal.
Billet	20.4	12.3	3.5	3.5	2.7	4.3	1.5	1.5	0.045	0.027	0.05	Bal.

Table II. LSHR Flow-Curve Observations

T, K (°C)	0.0005 s^{-1}	0.01 s^{-1}	0.1 s^{-1}	1 s^{-1}
1144 (871)	FS	FS	--	--
1283 (1010)	FS/MFS	FS	--	FS
1311 (1038)	SS	--	FS	FS
1339 (1066)	SS/MFH	FS	FS	FS
1366 (1093)	MFH	--	FS	FS
1408 (1135)	FH	SS/MFS	FS	FS
1450 (1177)	SS/FS	SS	FS	FS

FS ≡ flow softening
MFS ≡ moderate flow softening (≤ approx. 15 pct.)
SS ≡ steady-state flow
MFH ≡ moderate flow hardening (≤ approx. 15 pct.)
FH ≡ flow hardening

Table III. LSHR Strain-Rate-Sensitivity Data from 0.0005 ↔ 0.001 s^{-1} Jump Tests*

Material	Location	T, K (°C)	m (ε ~ 0.15)	m (ε ~ 0.85)
Pancake	--	1144 (871)	0.16	0.22
230-mm ϕ Billet	ID	1144 (871)	0.16	0.27
230-mm ϕ Billet	OD	1144 (871)	0.21	0.25
75-mm ϕ Billet	ID	1144 (871)	0.13	0.27
75-mm ϕ Billet	OD	1144 (871)	0.14	0.24
Pancake	--	1283 (1010)	--	--
230-mm ϕ Billet	ID	1283 (1010)	0.61	0.65
230-mm ϕ Billet	OD	1283 (1010)	0.60	0.60
Pancake	--	1339 (1066)	0.75	0.70
230-mm ϕ Billet	ID	1339 (1066)	0.60	0.64
230-mm ϕ Billet	OD	1339 (1066)	0.55	0.55
75-mm ϕ Billet	ID	1339 (1066)	0.69	0.69
75-mm ϕ Billet	OD	1339 (1066)	0.68	0.68
Pancake	--	1408 (1135)	0.63	0.47
230-mm ϕ Billet	ID	1408 (1135)	0.61	0.51
230-mm ϕ Billet	OD	1408 (1135)	0.61	0.47
Pancake	--	1450 (1177)	0.30	0.23
230-mm ϕ Billet	ID	1450 (1177)	0.41	0.33
230-mm ϕ Billet	OD	1450 (1177)	0.44	0.38

* Preheat (soak) time was 10 minutes for all experiments.

Table IV. LSHR Grain-Size Data*

Material	Defm Temp, K (°C)	$\dot{\varepsilon}$ (s^{-1})	As-Defm GS/ALA (μm)	Defm + HT GS/ALA (μm)
Pancake	1144 (871)	0.0005	~1.0/2.0	15.8/28.8
230-mm Billet	1283 (1010)	0.0005	1.5/11.8	16.5/78.8
230-mm Billet	1283 (1010)	0.01	1.2/7.8	13.3/64.1
230-mm Billet	1283 (1010)	1	1.0/13.3	13.2/74.3
Pancake	1339 (1066)	0.0005	2.4/10.3	19.1/73.2
230-mm Billet	1339 (1066)	0.0005	2.1/7.3	15.5/67.9
230-mm Billet	1339 (1066)	0.01	1.7/6.4	12.8/48.9
230-mm Billet	1339 (1066)	1.0	1.1/15.4	13.6/48.6
Pancake	1408 (1135)	0.0005	7.2/29.4	78.5/314.6
230-mm Billet	1408 (1135)	0.0005	5.9/17.1	31.5/269.7
230-mm Billet	1408 (1135)	0.01	2.8/13.1	55.8/246.8
Pancake	1450 (1177)	0.0005	22.7/138	---
230-mm Billet	1450 (1177)	0.0005	16.1/48.9	16.2/55.4
230-mm Billet	1450 (1177)	0.01	14.7/75.6	31.8/184.1

* As-deformed subsolvus data are averages of gamma and gamma-prime grain size. Preheat time prior to deformation was 10 minutes. Post compression heat treatment was 1444 K (1171°C) for 1 h.

Table V. LSHR Gamma Grain-Size Data: Samples Compressed at 0.0005 s^{-1}

Material	Temp(K)/ Time (min)	As-Defm GS/ALA (μm)	2140F/30 min GS/ALA (μm)	2140F/1h GS/ALA (μm)	2140F/2h GS/ALA (μm)
Pancake	1339/10	2.4/10.3	---	19.1/73.2	19.8/79.0
Pancake	1339/60	---	---	17.5/60.6	---
Pancake	1408/10	7.2/29.4	77.3/356.0	78.5/314.6	81.3/352.2
Pancake	1408/60	---	---	101.6/418.6	---
230-mm Billet	1339/10	2.1/7.3	---	15.5/67.9	15.7/65.2
230-mm Billet	1339/60	---	---	15.0/76.9	---
230-mm Billet	1408/10	5.9/17.1	23.9/292.7	31.5/269.7	20.1/276.2
230-mm Billet	1408/60	---	---	37.2/244.3	---

Figure Captions

Figure 1. True stress-true strain curves obtained from constant-strain-rate compression tests on LSHR pancake conducted at test temperatures of: (a) 1339 K (1066°C), (b) 1408 K (1135°C), and (c) 1450 K (1177°C). The soak time at temperature prior to deformation was 10 minutes.

Figure 2. True stress-true strain curves obtained from constant-strain-rate compression tests on samples taken from the outer-diameter of 230-mm-diameter LSHR billet conducted at test temperatures of: (a) 1339 K (1066°C), (b) 1408 K (1135°C), and (c) 1450 K (1177°C). The soak time at temperature prior to deformation was 10 minutes.

Figure 3. Effect of test temperature on stress-strain response at a constant strain rate of 0.0005 s^{-1} for samples extracted from (a) LSHR pancake or (b) the outer-diameter of 230-mm-diameter LSHR billet. The soak time at temperature prior to deformation was 10 minutes.

Figure 4. True stress-true strain curves obtained from constant-strain-rate compression tests on samples taken from 230-mm-diameter LSHR billet illustrating the effect on plastic-flow behavior of: (a) soak (preheat) time (for OD samples) and (b, c) radial location within the billet (i.e., OD vs ID). For the data in b, c, the soak time at temperature prior to deformation was 10 minutes.

Figure 5. Log-log plots of flow stress at a strain of ~0.01 versus strain rate for (a) LSHR pancake and (b) OD samples of 230-mm-diameter LSHR billet.

Figure 6. Backscattered electron micrographs of LSHR pancake samples which were water quenched following a 10 minute soak at a temperature of (a) 1144 K (871°C), (b) 1311 K (1038°C), (c) 1339 K (1066°C), (d) 1366 K (1093°C), (e) 1408 K (1135°C), or (f) 1450 K (1177°C).

Figure 7. Backscattered electron micrographs of LSHR pancake samples which were forced-air cooled following isothermal, hot compression to a 2:1 height reduction at a strain rate of 0.0005 s^{-1} and test temperature of (a) 1144 K (871°C), (b) 1339 K (1066°C), (c) 1408 K (1135°C), or (d) 1450 K (1177°C). The soak time at temperature prior to deformation was 10 minutes.

Figure 8. Backscattered electron micrographs of LSHR pancake samples illustrating the degree of dynamic grain growth during a 2:1 height reduction at a strain rate of 0.0005 s^{-1}: (a) Preheated 10 minutes at 1339 K (1066°C), (b) preheated 10 minutes and deformed at 1339 K (1066°C), (c) preheated 10 minutes at 1408 K (1135°C), (d) preheated 10 minutes and deformed at 1408 K (1135°C), (e) preheated 60 minutes at 1408 K (1135°C), (f) preheated 60 minutes and deformed at 1408 K (1135°C).

Figure 9. Backscattered electron images illustrating the as-deformed microstructures developed in 230-mm-diameter LSHR-extrusion OD samples compressed to a 2:1 height reduction at various strain rates and test temperatures of (a, b, c) 1339 K (1066°C) or (d, e) 1408 K (1135°C). The soak time at temperature prior to deformation was 10 minutes.

Figure 10. Backscattered electron micrographs of LSHR pancake samples which were supersolvus heat treated at 1444 K (1171°C) for 1 h following isothermal, hot

compression to a 2:1 height reduction at a strain rate of 0.0005 s^{-1} and test temperature of (a) 1144 K (871°C), (b) 1339 K (1066°C), (c) 1408 K (1135°C), or (d) 1450 K (1177°C). The soak time at temperature prior to deformation was 10 minutes.

Figure 11. Backscattered electron images illustrating the microstructures developed in 230-mm-diameter LSHR-extrusion OD samples which were supersolvus heat treated at 1444 K (1171°C) for 1 h following compression to a 2:1 height reduction at various strain rates and test temperatures of (a, b, c) 1339 K (1066°C) or (d, e) 1408 K (1135°C). The soak time at temperature prior to deformation was 10 minutes.

Figure 12. EBSD-determined grain structures for LSHR pancake samples which were preheated 10 minutes and compressed to a 2:1 reduction at 0.0005 s^{-1} and temperatures of (a) 1339 K (1066°C) or (b) 1408 K (1135°C). High-angle grain boundaries are indicated in black. Sub-boundaries with misorientations of 2-3°, 3-5°, 5-10°, or 10-15° are indicated with red, green, blue, or yellow lines, respectively. All twin boundaries have been removed.

Figure 13. EBSD data for (a, b) Grain average misorientation (GAM), (c, d) grain-reference-orientation deviation (GROD), and (e, f) grain-orientation spread (GOS) developed in LSHR pancake samples which were preheated 10 minutes and compressed to a 2:1 reduction at 0.0005 s^{-1} and a temperature of (a, c, e) 1339 K (1066°C) or (b, d, f) 1408 K (1135°C).

Figure 14. EBSD determinations of (a, b) 100 pole figures and (c, d) grain-boundary misorientation distributions (neglecting twin boundaries) for LSHR pancake

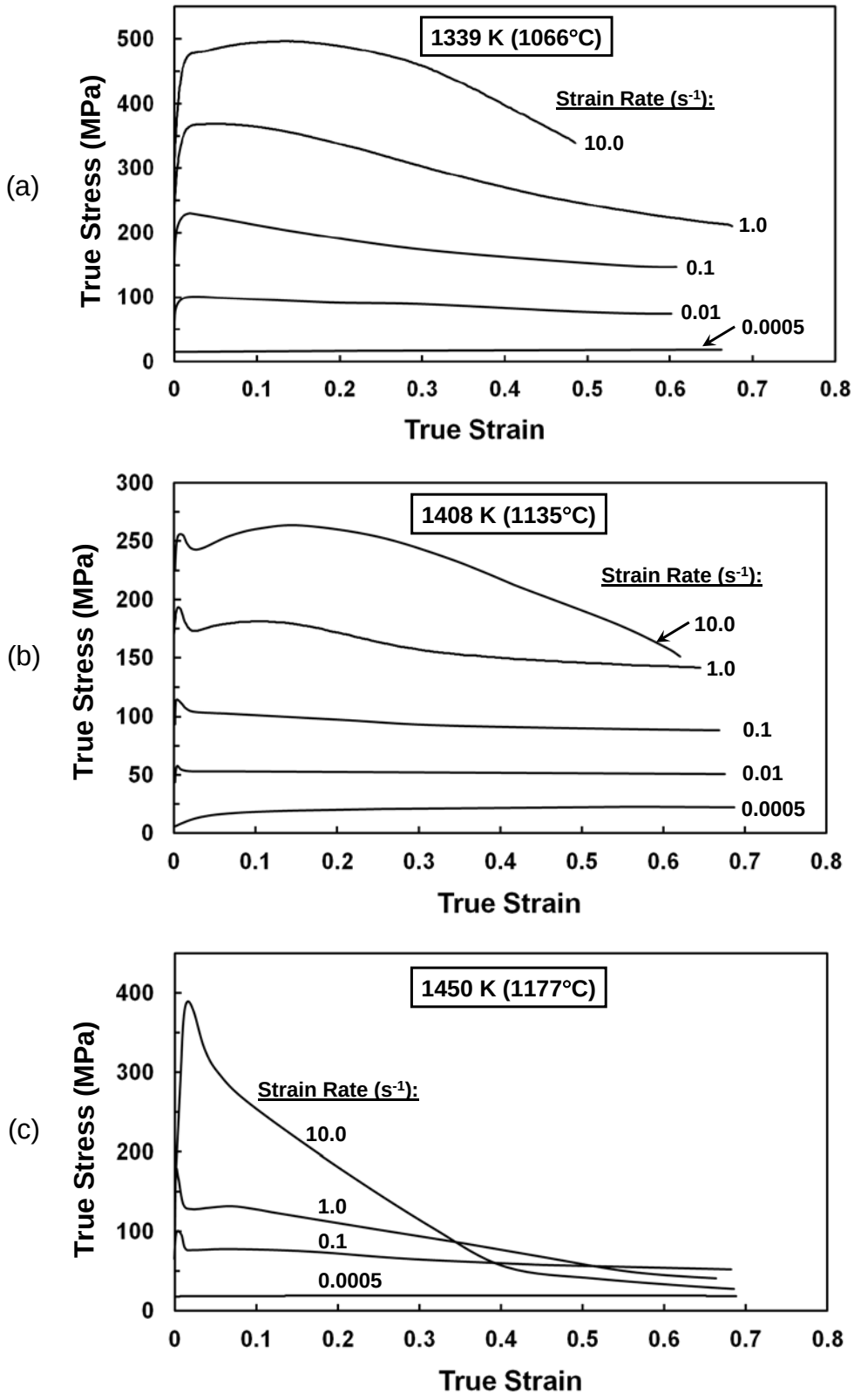

Figure 1. True stress-true strain curves obtained from constant-strain-rate compression tests on LSHR pancake conducted at test temperatures of: (a) 1339 K (1066°C), (b) 1408 K (1135°C), and (c) 1450 K (1177°C). The soak time at temperature prior to deformation was 10 minutes.

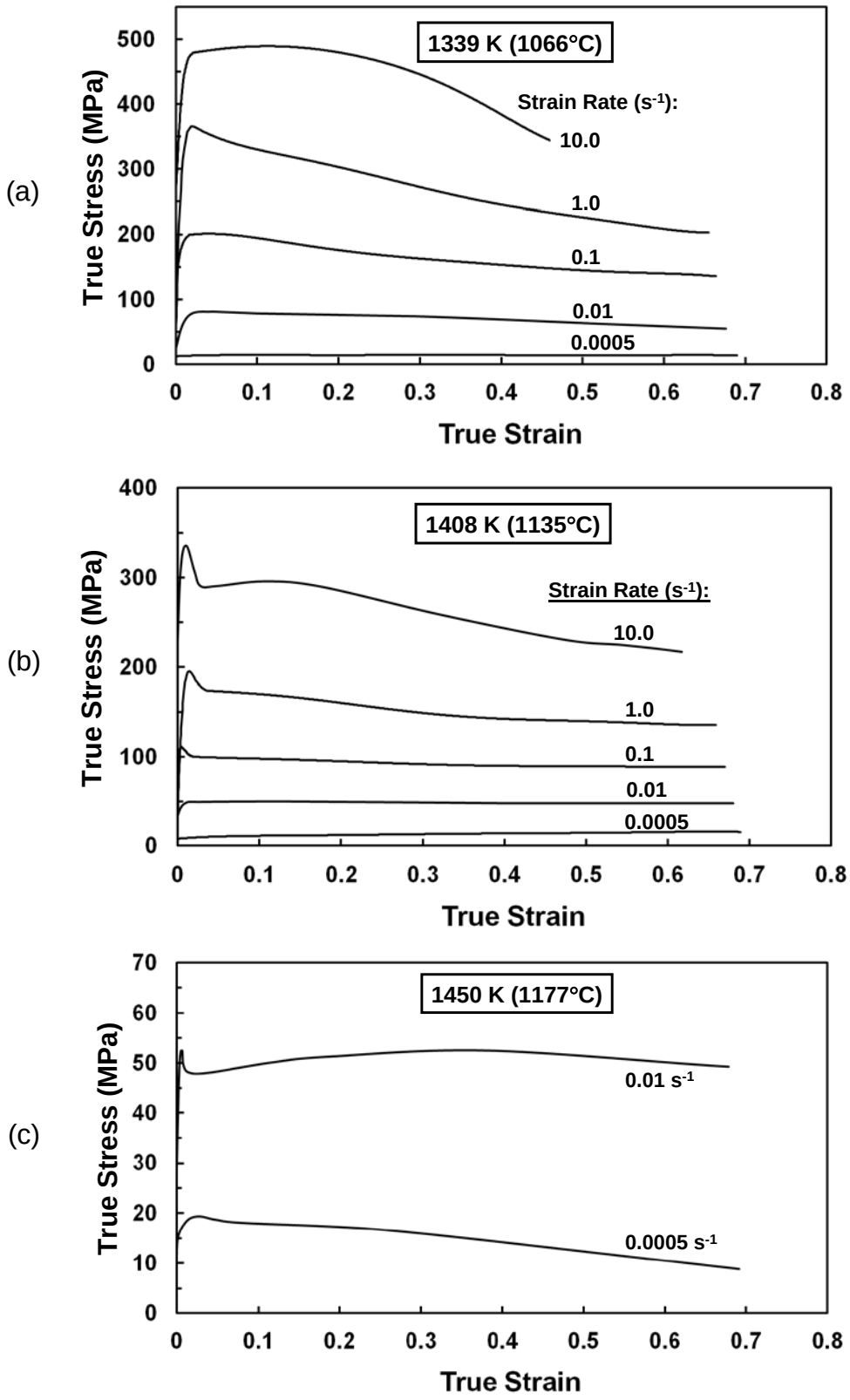

Figure 2. True stress-true strain curves obtained from constant-strain-rate compression tests on samples taken from the outer-diameter of 230-mm-diameter LSHR billet conducted at test temperatures of: (a) 1339 K (1066°C), (b) 1408 K (1135°C), and (c) 1450 K (1177°C). The soak time at temperature prior to deformation was 10 minutes.

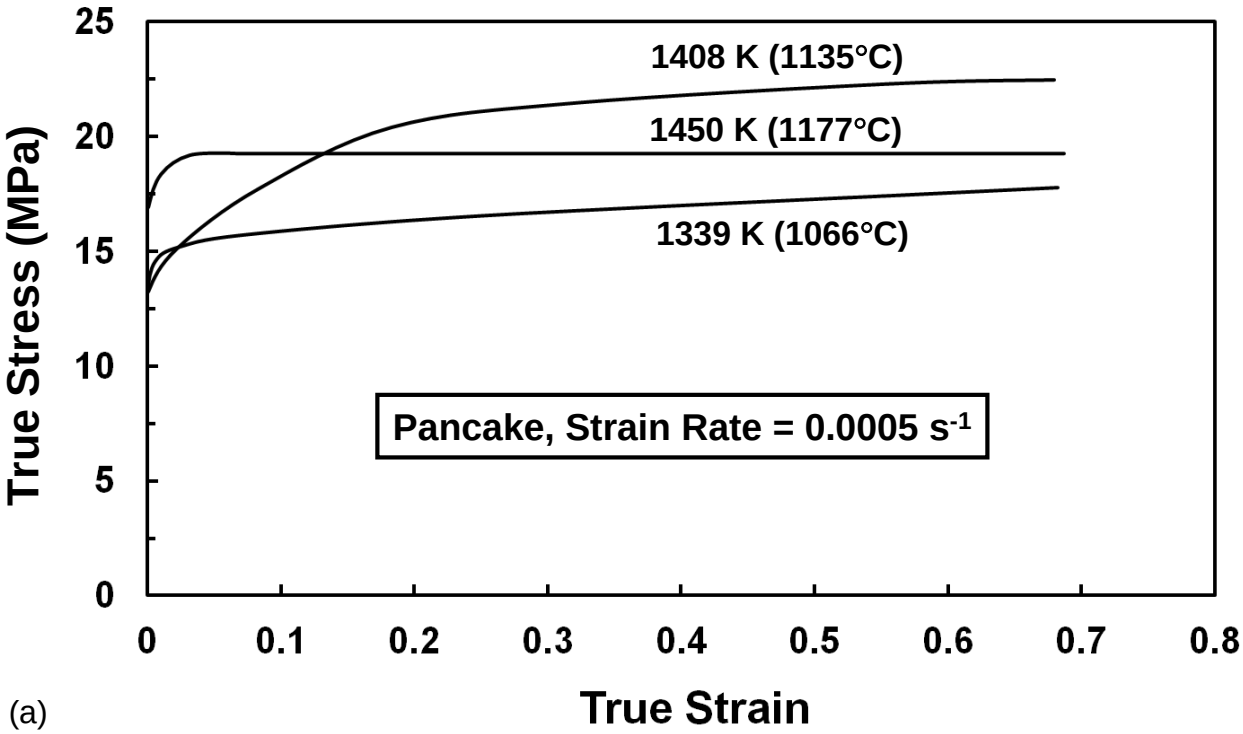

(a)

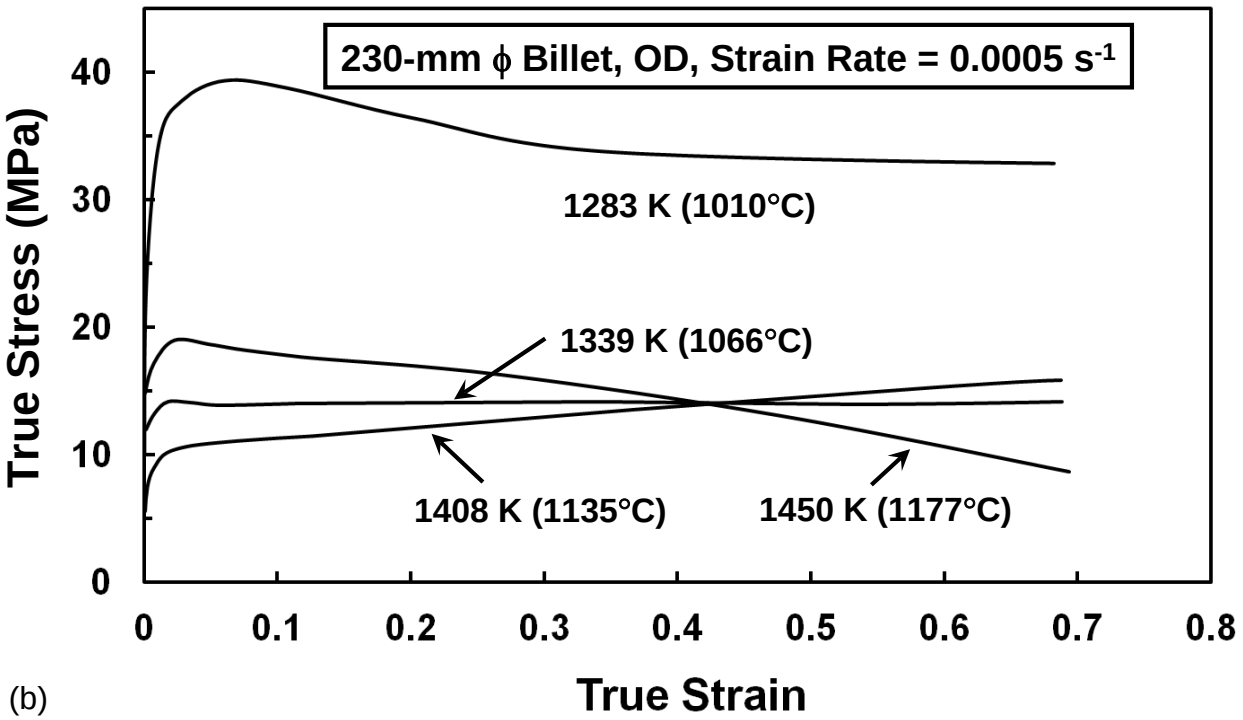

(b)

Figure 3. Effect of test temperature on stress-strain response at a constant strain rate of 0.0005 s^{-1} for samples extracted from (a) LSHR pancake or (b) the outer-diameter of 230-mm-diameter LSHR billet. The soak time at temperature prior to deformation was 10 minutes.

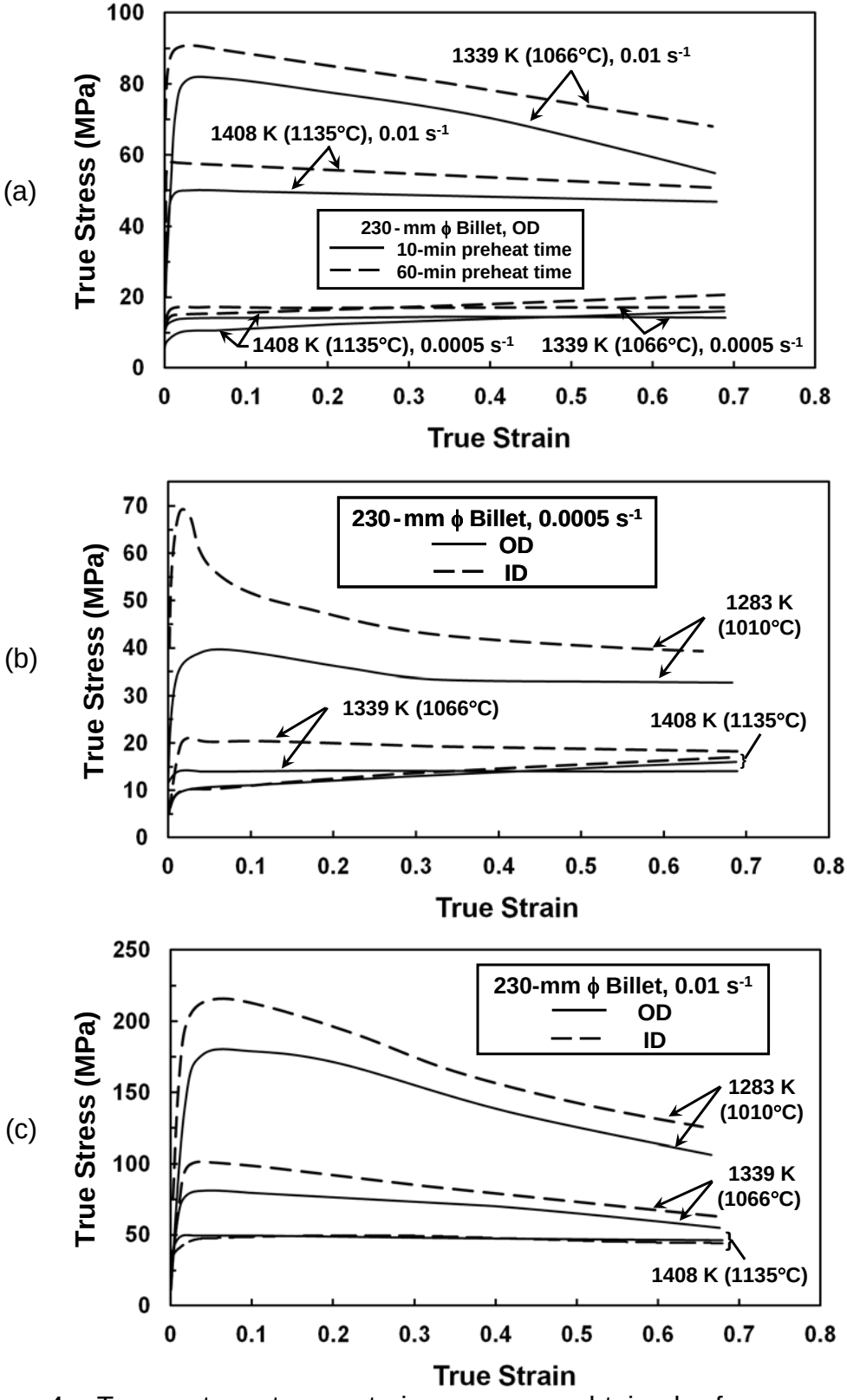

Figure 4. True stress-true strain curves obtained from constant-strain-rate compression tests on samples taken from 230-mm-diameter LSHR billet illustrating the effect on plastic-flow behavior of: (a) soak (preheat) time (for OD samples) and (b, c) radial location within the billet (i.e., OD vs ID). For the data in b, c, the soak time at temperature prior to deformation was 10 minutes.

(a)

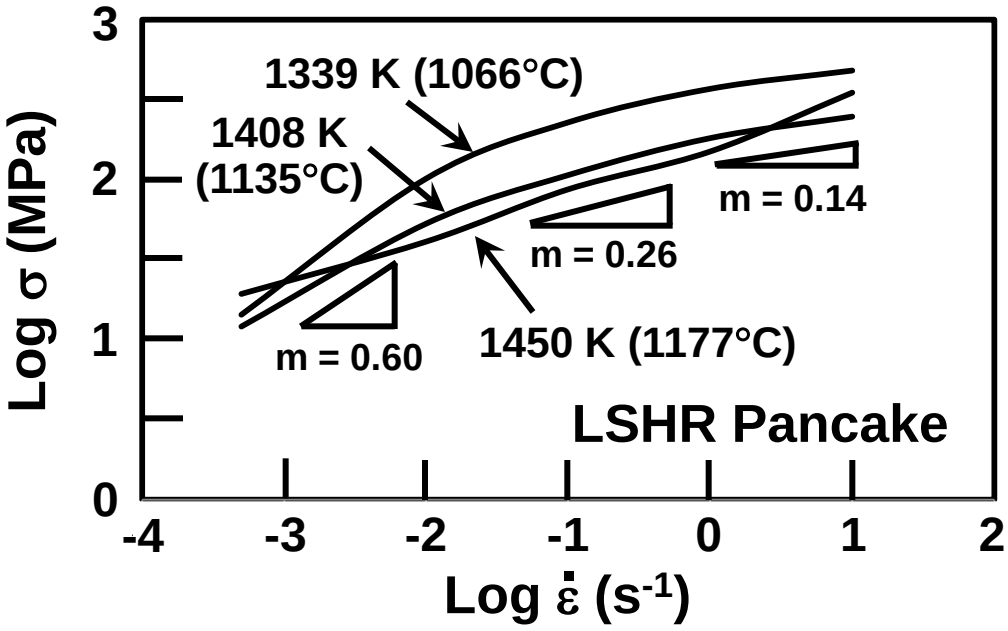

(b)

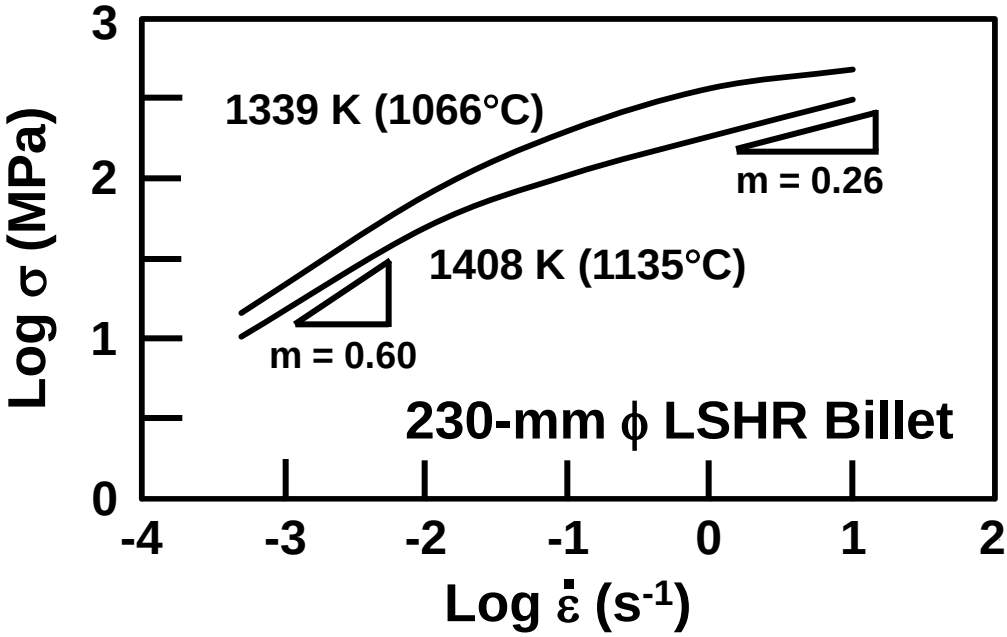

Figure 5. Log-log plots of flow stress at a strain of ~0.01 versus strain rate for (a) LSHR pancake and (b) OD samples of 230-mm-diameter LSHR billet.

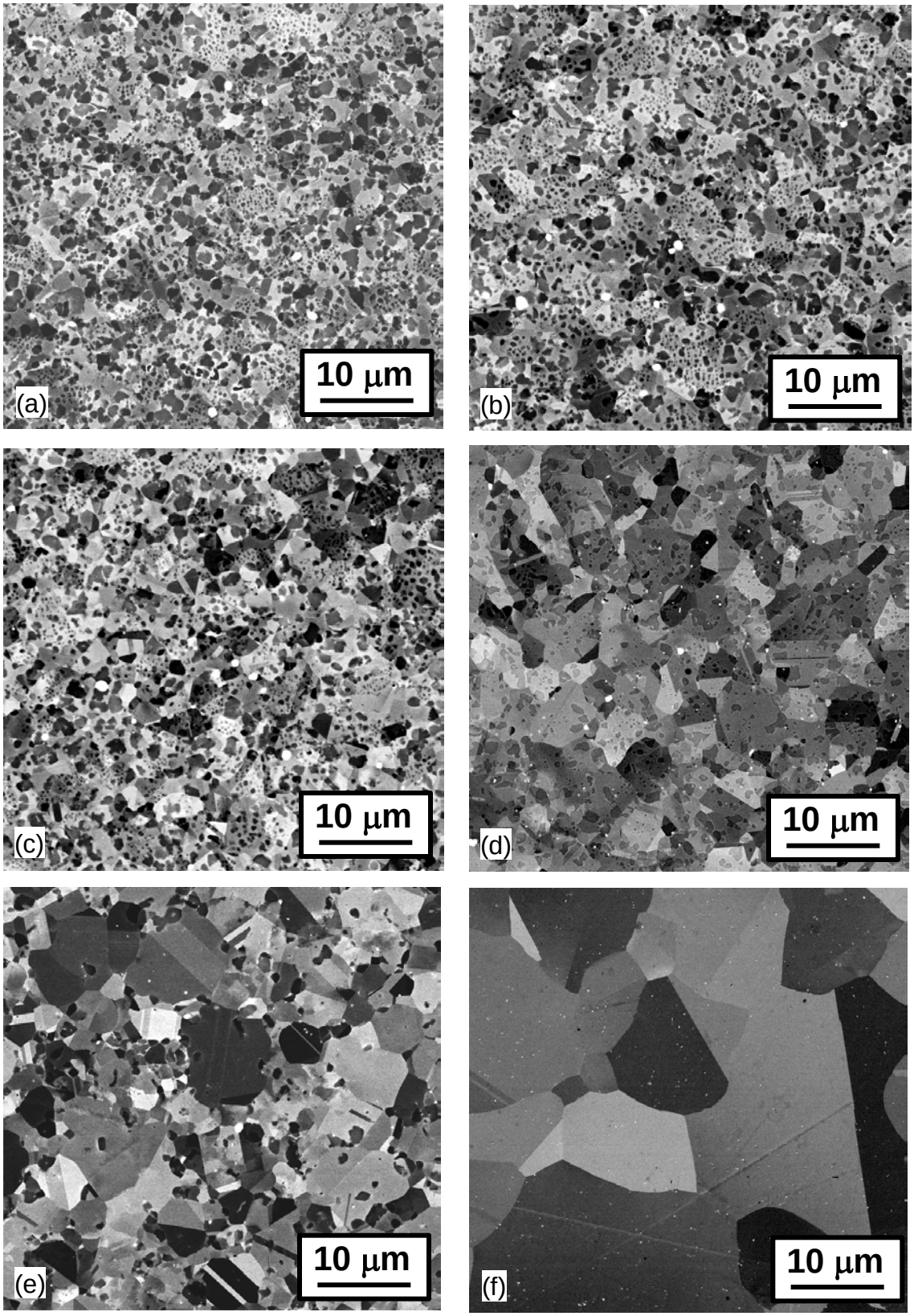

Figure 6. Backscattered electron micrographs of LSHR pancake samples which were water quenched following a 10 minute soak at a temperature of (a) 1144 K (871°C), (b) 1311 K (1038°C), (c) 1339 K (1066°C), (d) 1366 K (1093°C), (e) 1408 K (1135°C), or (f) 1450 K (1177°C).

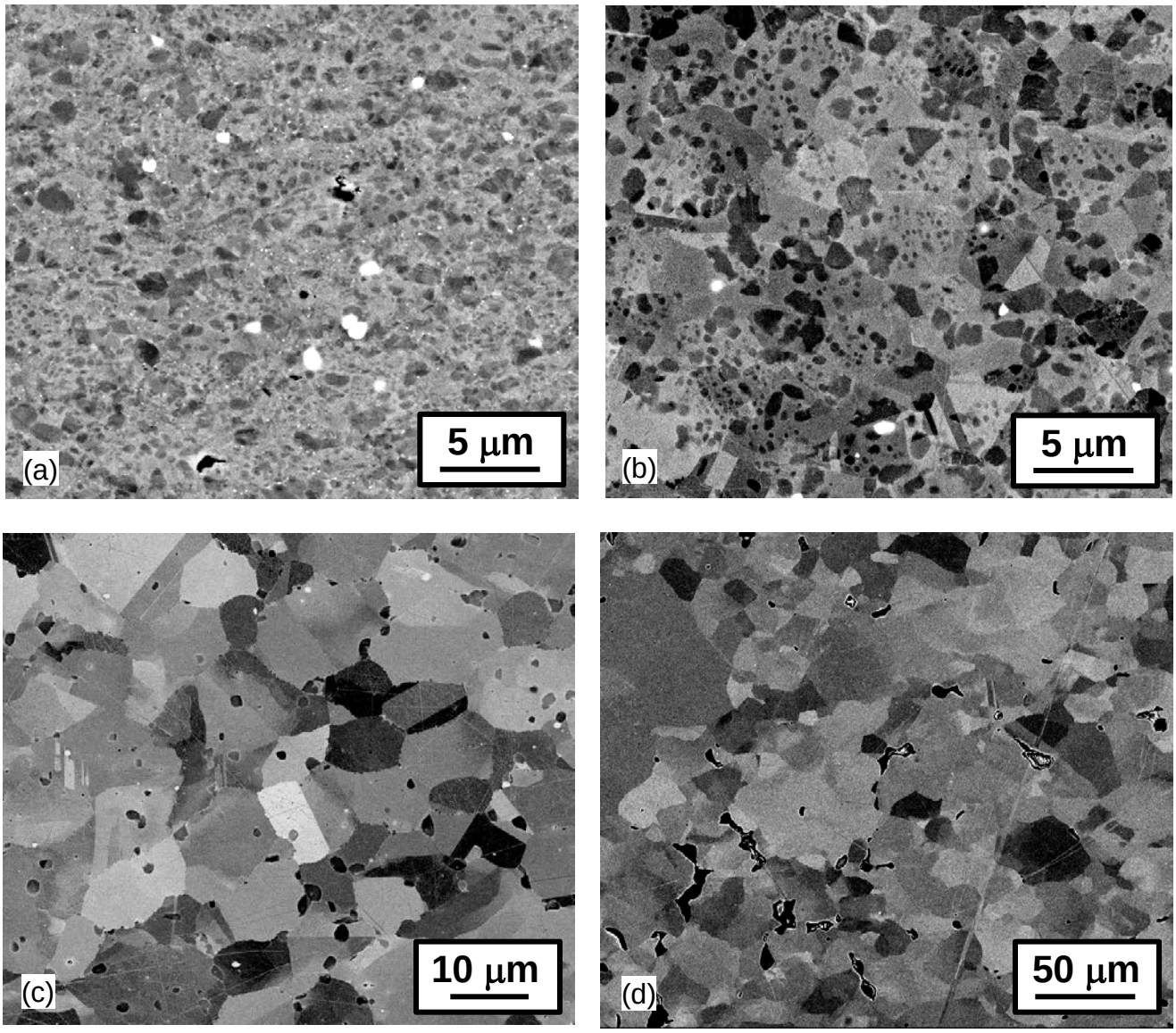

Figure 7. Backscattered electron micrographs of LSHR pancake samples which were forced-air cooled following isothermal, hot compression to a 2:1 height reduction at a strain rate of 0.0005 s^{-1} and test temperature of (a) 1144 K (871°C), (b) 1339 K (1066°C), (c) 1408 K (1135°C), or (d) 1450 K (1177°C). The soak time at temperature prior to deformation was 10 minutes.

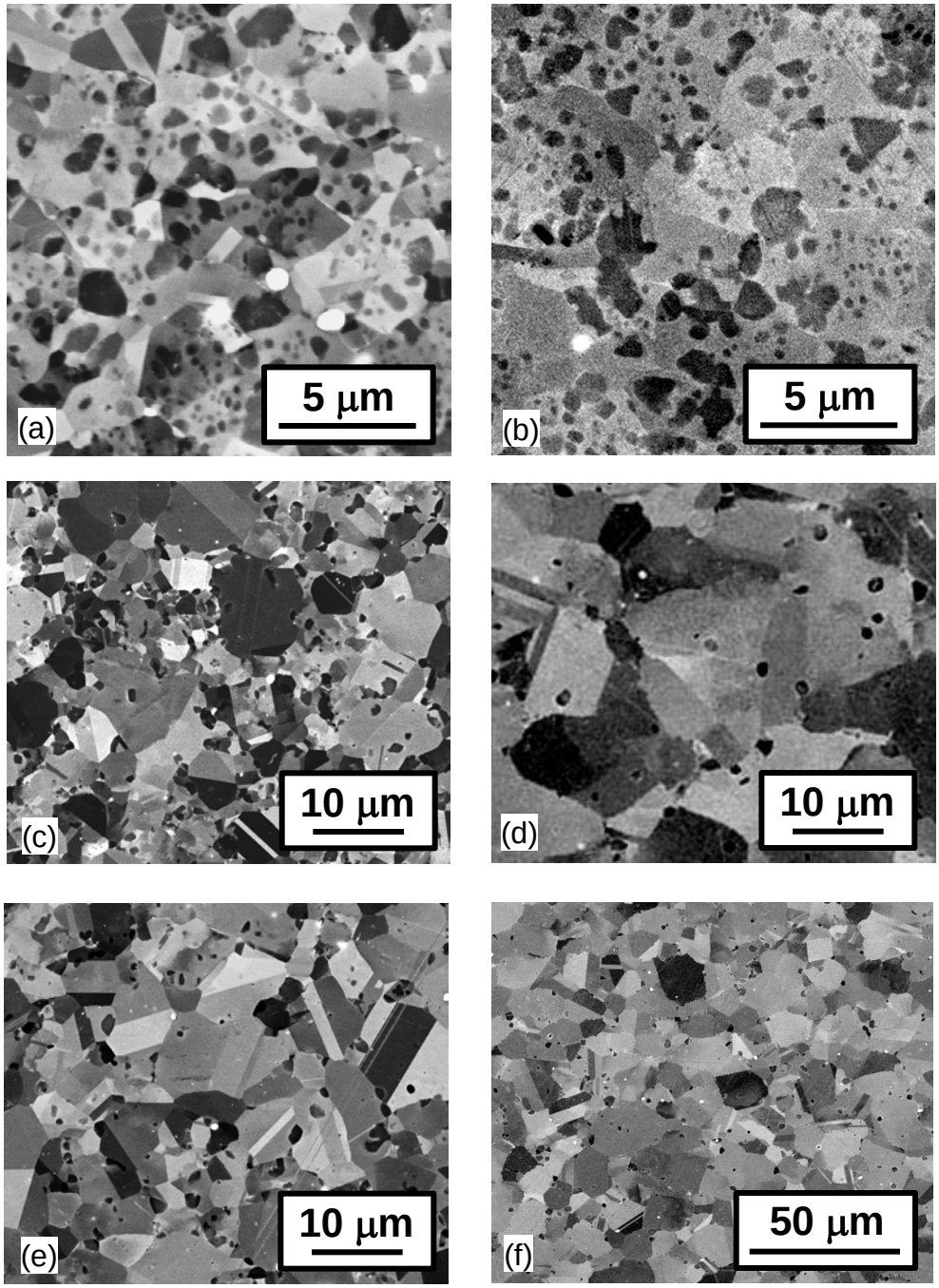

Figure 8. Backscattered electron micrographs of LSHR pancake samples illustrating the degree of dynamic grain growth during a 2:1 height reduction at a strain rate of 0.0005 s^{-1}: (a) Preheated 10 minutes at 1339 K (1066°C), (b) preheated 10 minutes and deformed at 1339 K (1066°C), (c) preheated 10 minutes at 1408 K (1135°C), (d) preheated 10 minutes and deformed at 1408 K (1135°C), (e) preheated 60 minutes at 1408 K (1135°C), (f) preheated 60 minutes and deformed at 1408 K (1135°C).

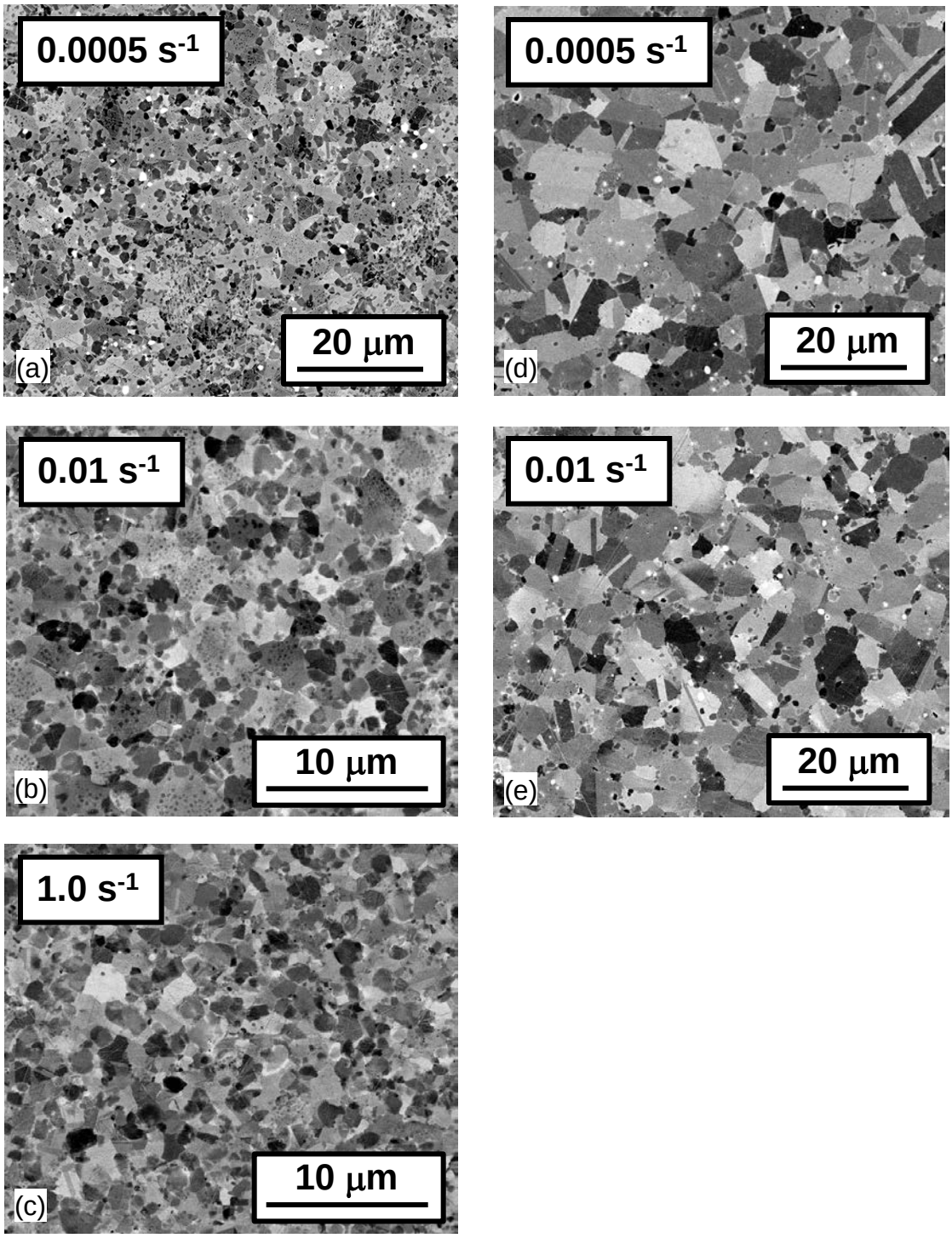

Figure 9. Backscattered electron images illustrating the as-deformed microstructures developed in 230-mm-diameter LSHR-extrusion OD samples compressed to a 2:1 height reduction at various strain rates and test temperatures of (a, b, c) 1339 K (1066°C) or (d, e) 1408 K (1135°C). The soak time at temperature prior to deformation was 10 minutes.

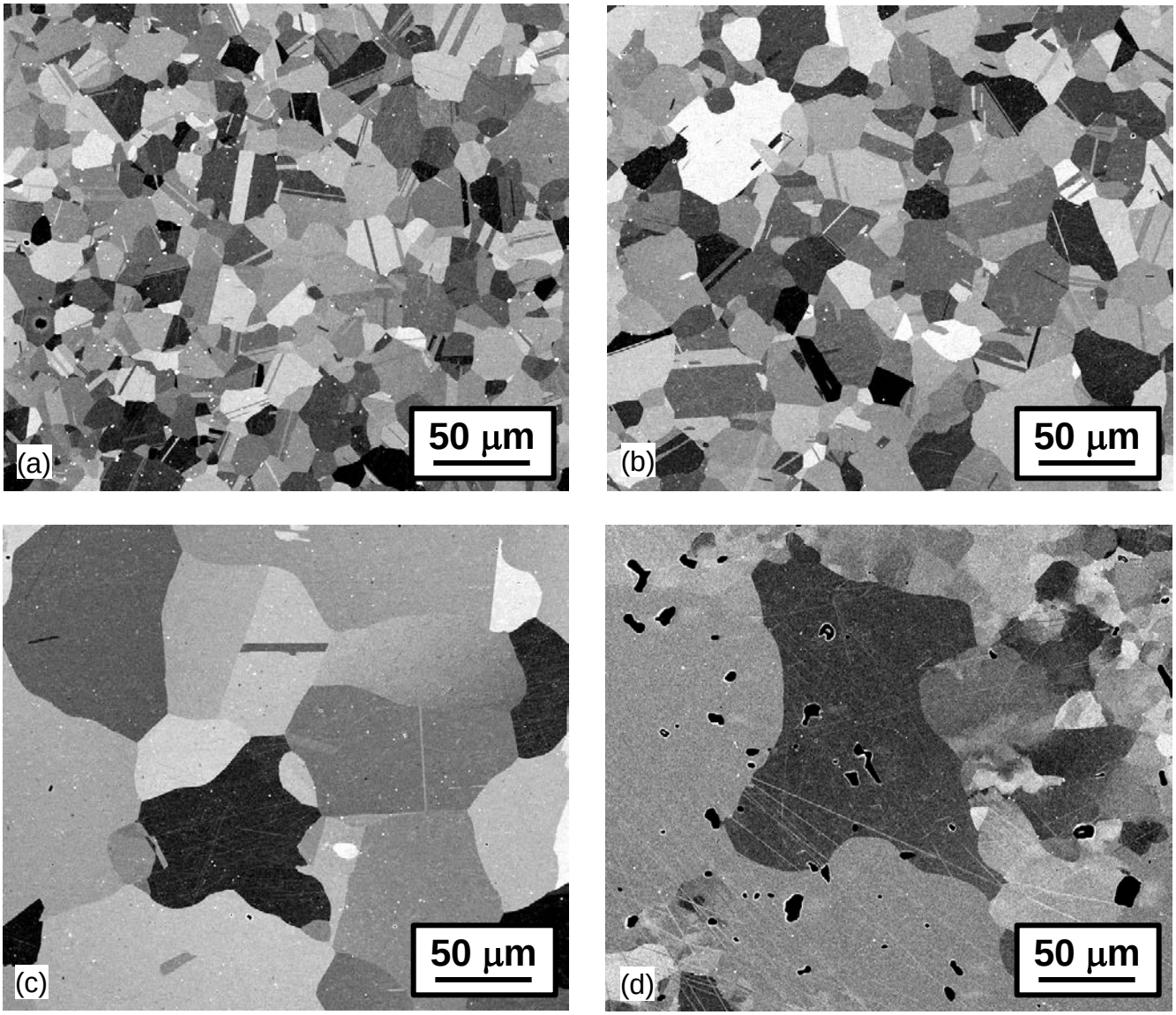

Figure 10. Backscattered electron micrographs of LSHR pancake samples which were supersolvus heat treated at 1444 K (1171°C) for 1 h following isothermal, hot compression to a 2:1 height reduction at a strain rate of 0.0005 s^{-1} and test temperature of (a) 1144 K (871°C), (b) 1339 K (1066°C), (c) 1408 K (1135°C), or (d) 1450 K (1177°C). The soak time at temperature prior to deformation was 10 minutes.

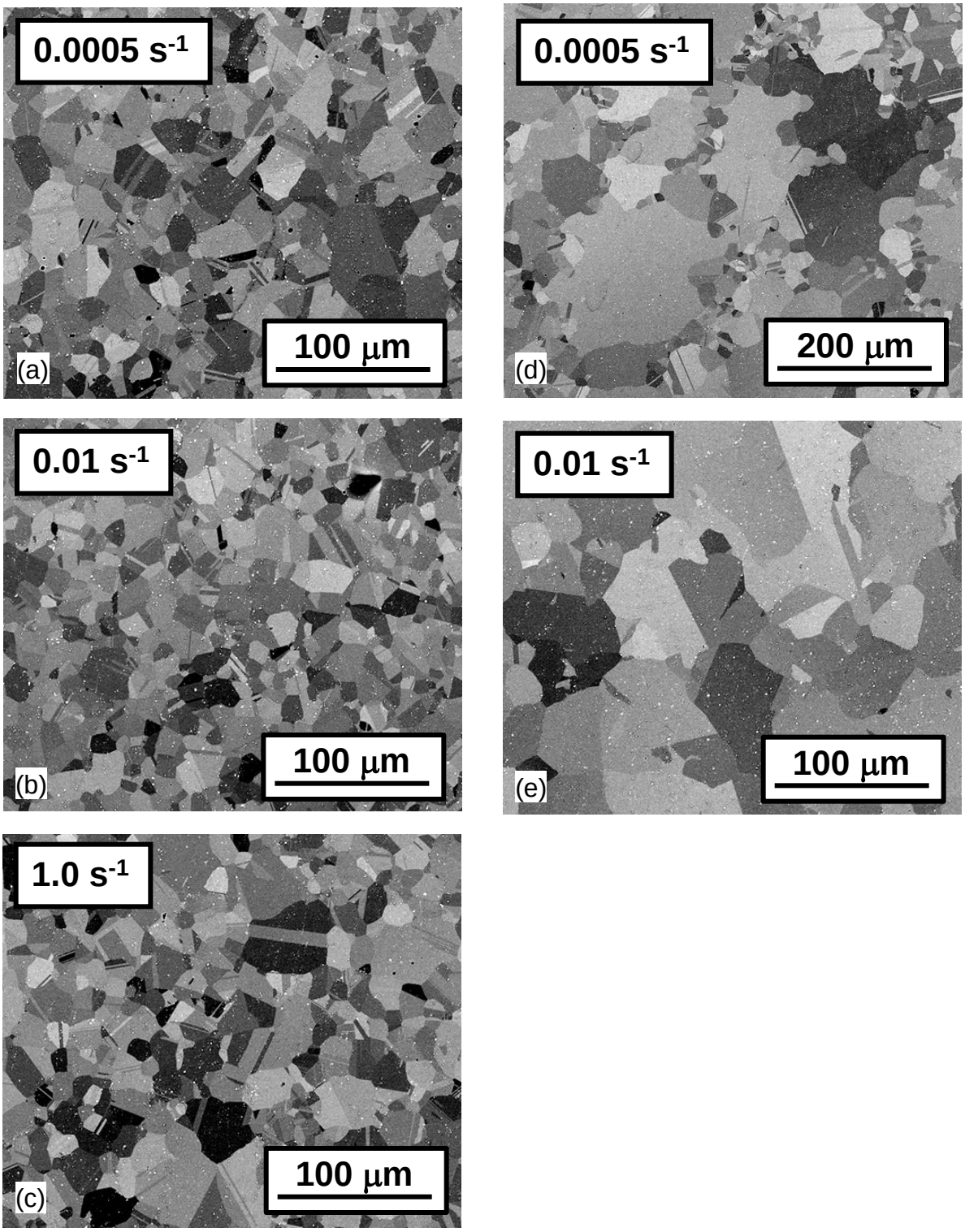

Figure 11. Backscattered electron images illustrating the microstructures developed in 230-mm-diameter LSHR-extrusion OD samples which were supersolvus heat treated at 1444 K (1171°C) for 1 h following compression to a 2:1 height reduction at various strain rates and test temperatures of (a, b, c) 1339 K (1066°C) or (d, e) 1408 K (1135°C). The soak time at temperature prior to deformation was 10 minutes.

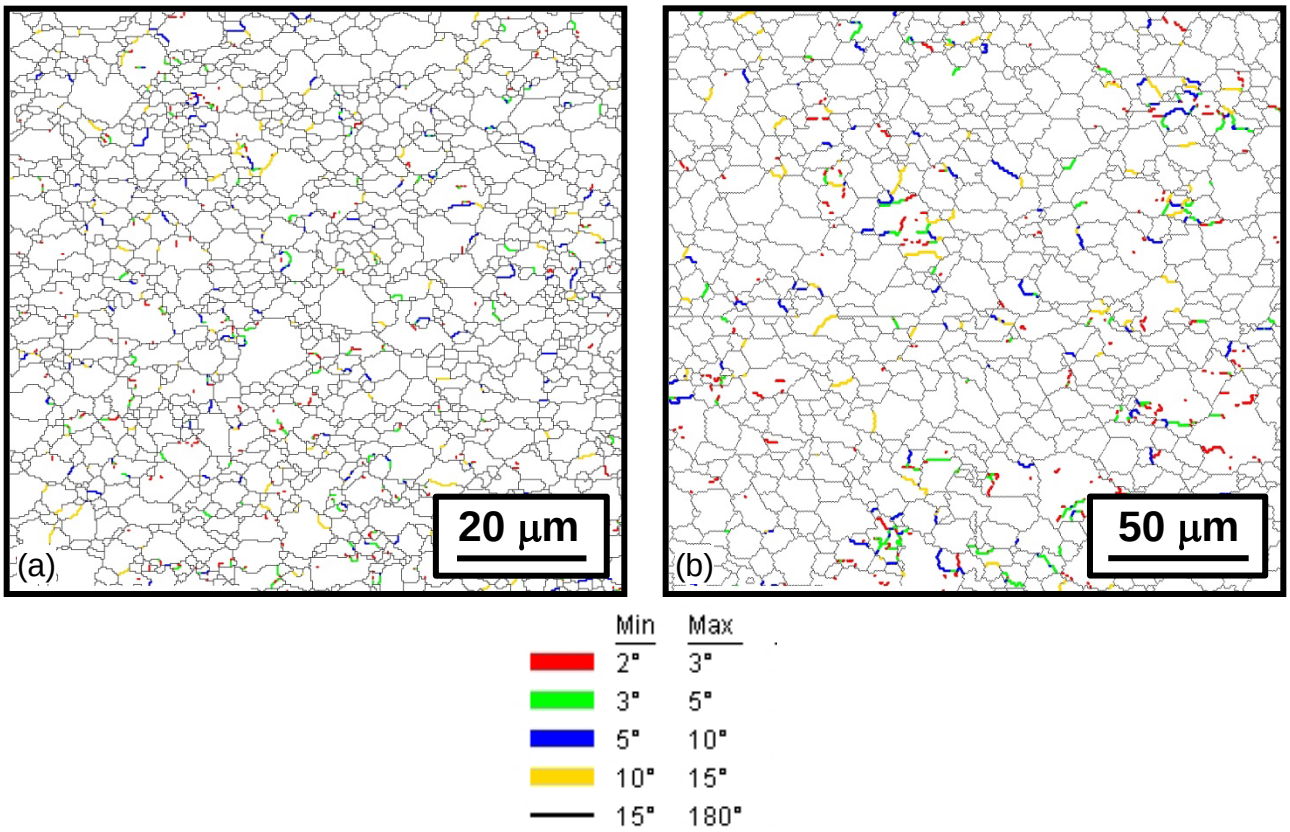

Figure 12. EBSD-determined grain structures for LSHR pancake samples which were preheated 10 minutes and compressed to a 2:1 reduction at 0.0005 s^{-1} and temperatures of (a) 1339 K (1066°C) or (b) 1408 K (1135°C). High-angle grain boundaries are indicated in black. Sub-boundaries with misorientations of 2-3°, 3-5°, 5-10°, or 10-15° are indicated with red, green, blue, or yellow lines, respectively. All twin boundaries have been removed.

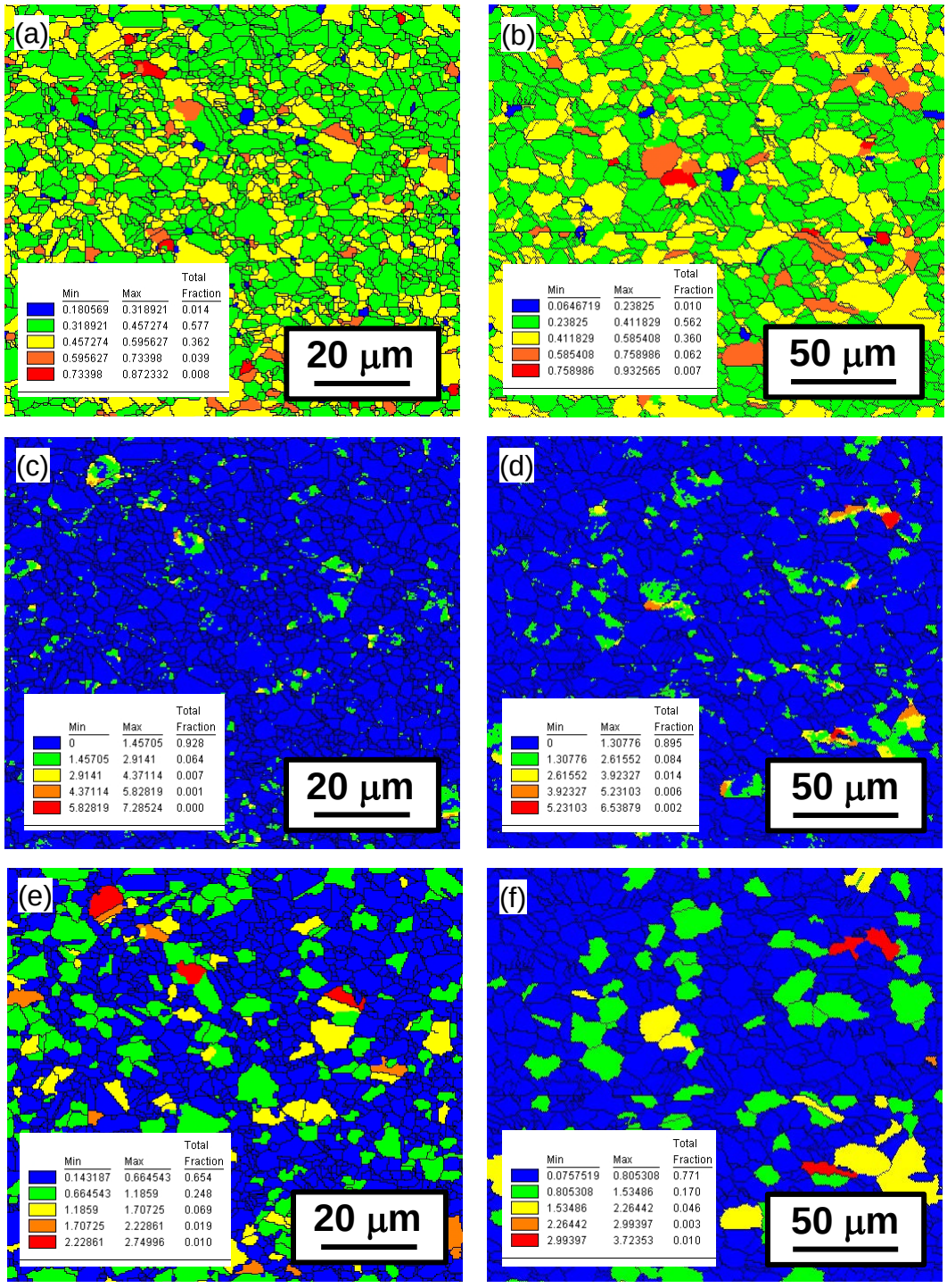

Figure 13. EBSD data for (a, b) Grain average misorientation (GAM), (c, d) grain-reference-orientation deviation (GROD), and (e, f) grain-orientation spread (GOS) developed in LSHR pancake samples which were preheated 10 minutes and compressed to a 2:1 reduction at 0.0005 s^{-1} and a temperature of (a, c, e) 1339 K (1066°C) or (b, d, f) 1408 K (1135°C).

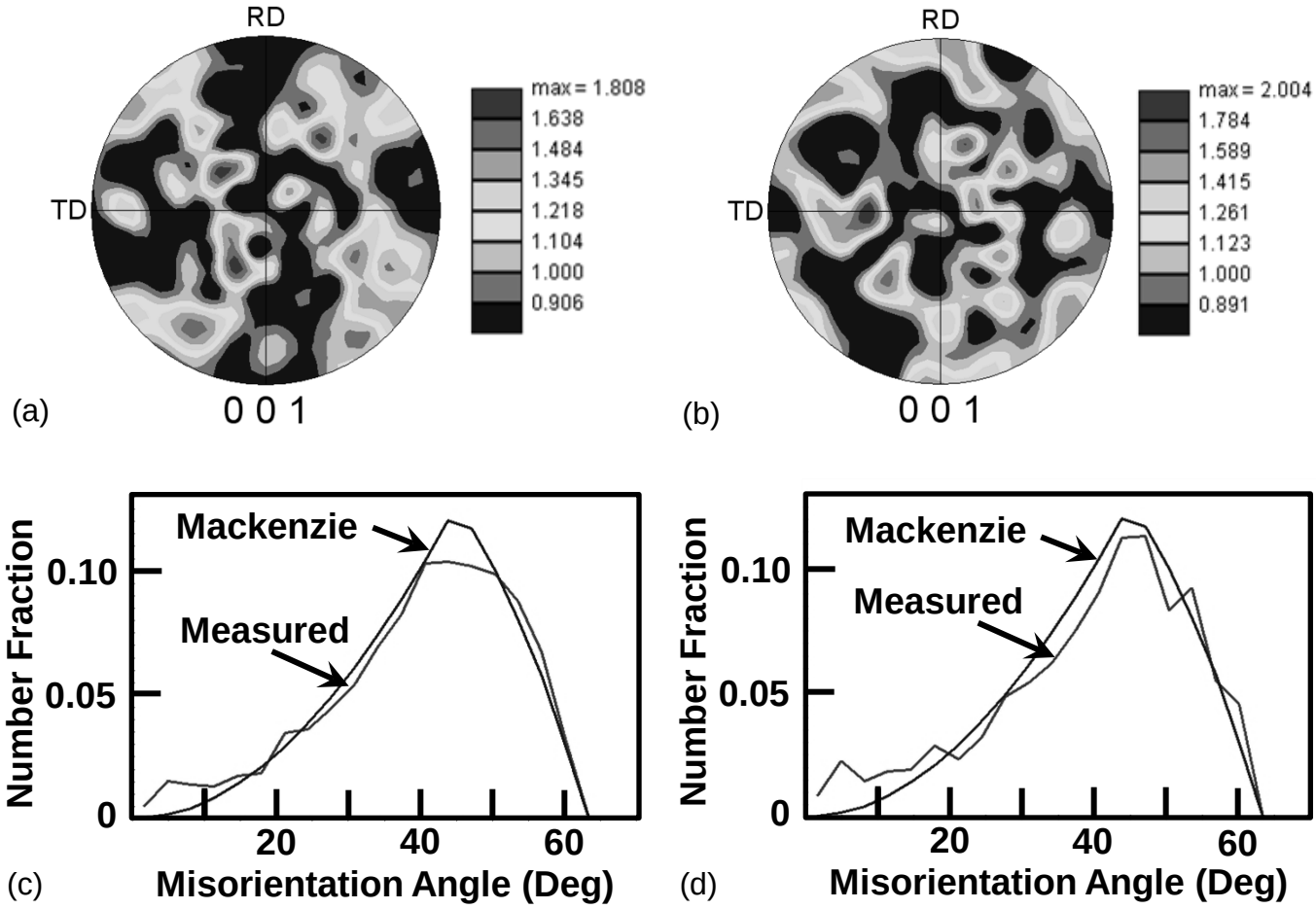

Figure 14. EBSD determinations of (a, b) 100 pole figures and (c, d) grain-boundary misorientation distributions (neglecting twin boundaries) for LSHR pancake samples which were preheated 10 minutes and compressed to a 2:1 reduction at 0.0005 s^{-1} and a temperature of (a, c) 1339 K (1066°C) or (b, d) 1408 K (1135°C).

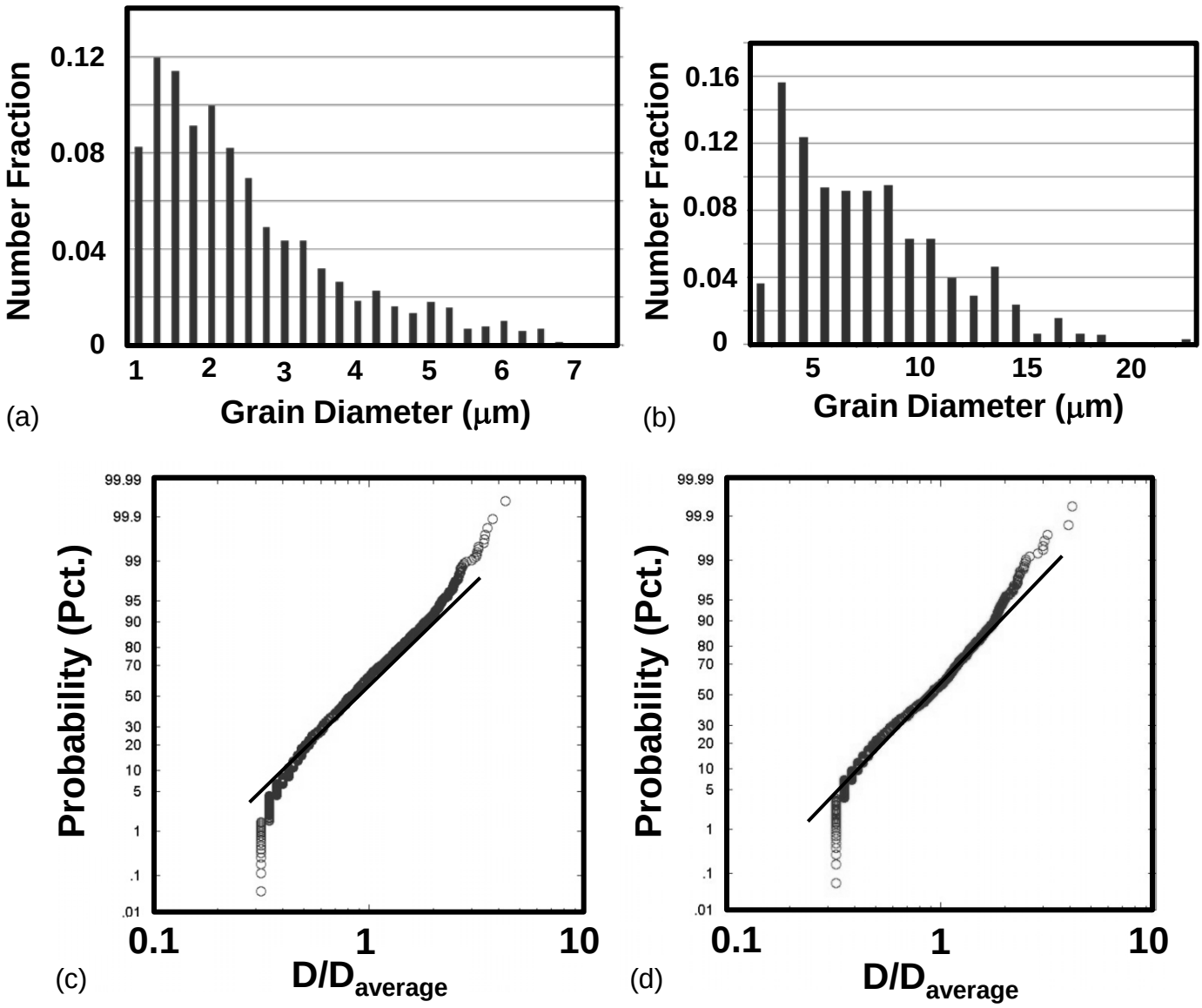

Figure 15. Grain-size data determined by EBSD represented in terms of (a, b) grain-size histograms and (c, d) probability plots of the normalized grain-size distribution for LSHR pancake samples which were preheated 10 minutes and compressed to a 2:1 reduction at 0.0005 s^{-1} and a temperature of (a, c) 1339 K (1066°C) or (b, d) 1408 K (1135°C).

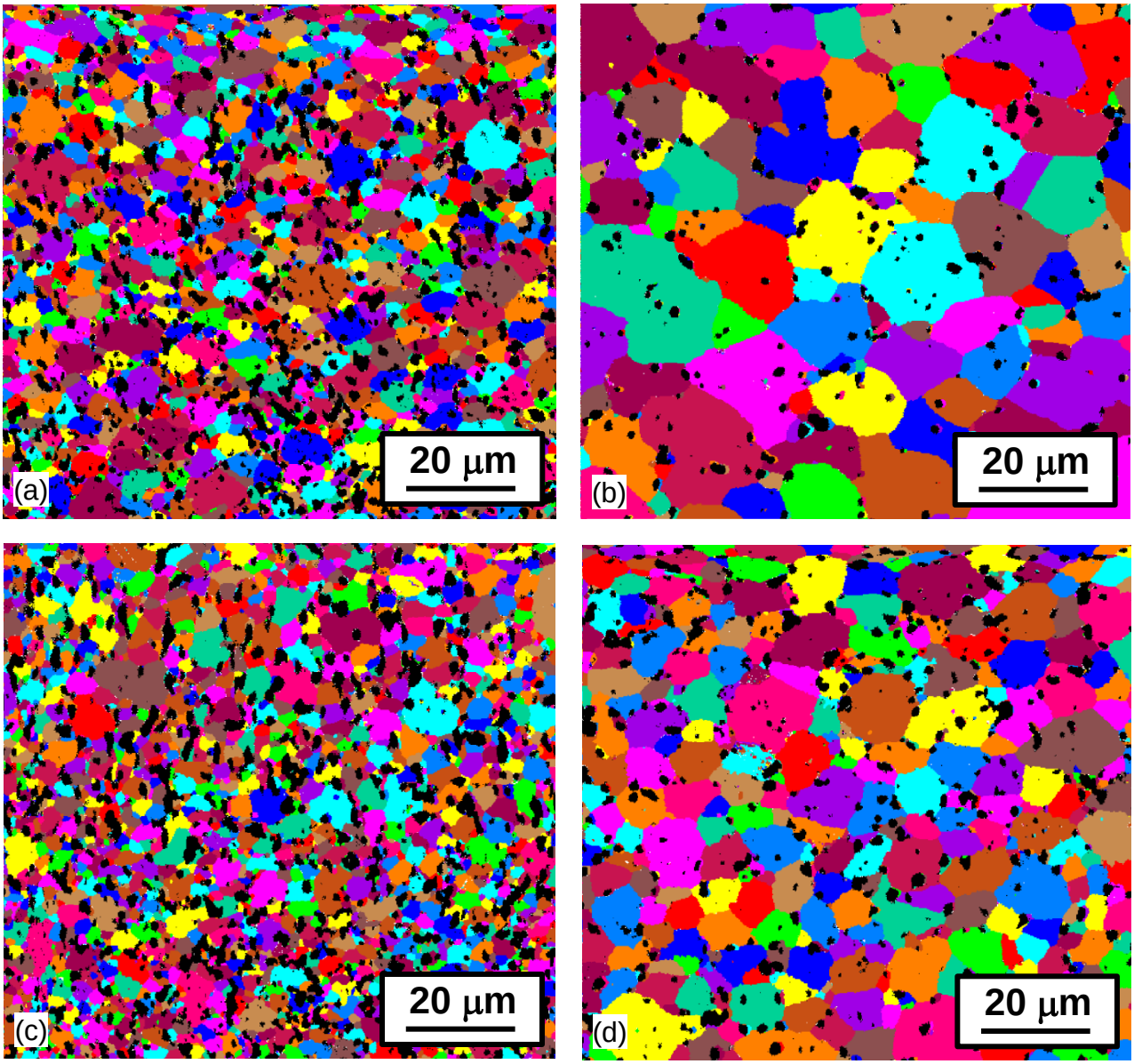

Figure 16. Gamma grains (colors) and gamma-prime precipitates (black particles) segmented via combined EBSD/EDS analysis of samples of (a, b) LSHR pancake or (c, d) 230-mm-diameter billet which were preheated 10 minutes and compressed to a 2:1 reduction at 0.0005 s^{-1} and a temperature of (a, c) 1339 K (1066°C) or (b, d) 1408 K (1135°C).

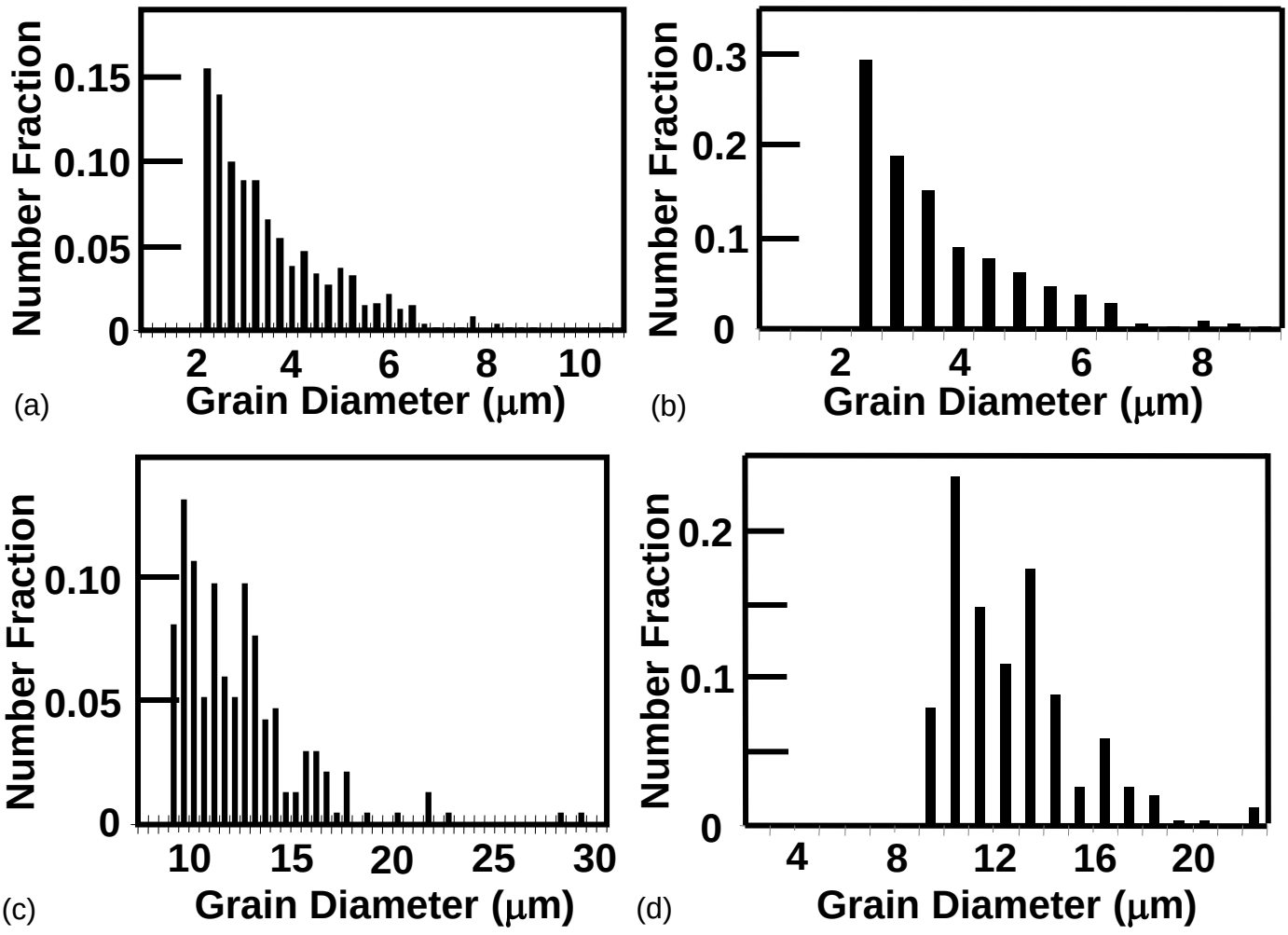

Figure 17. Approximate histograms of the gamma grain-size distribution extracted from segmented images of LSHR pancake samples which were preheated 10 minutes and compressed to a 2:1 reduction at 0.0005 s^{-1} and a temperature of (a, b) 1339 K (1066°C) or (c, d) 1408 K (1135°C).

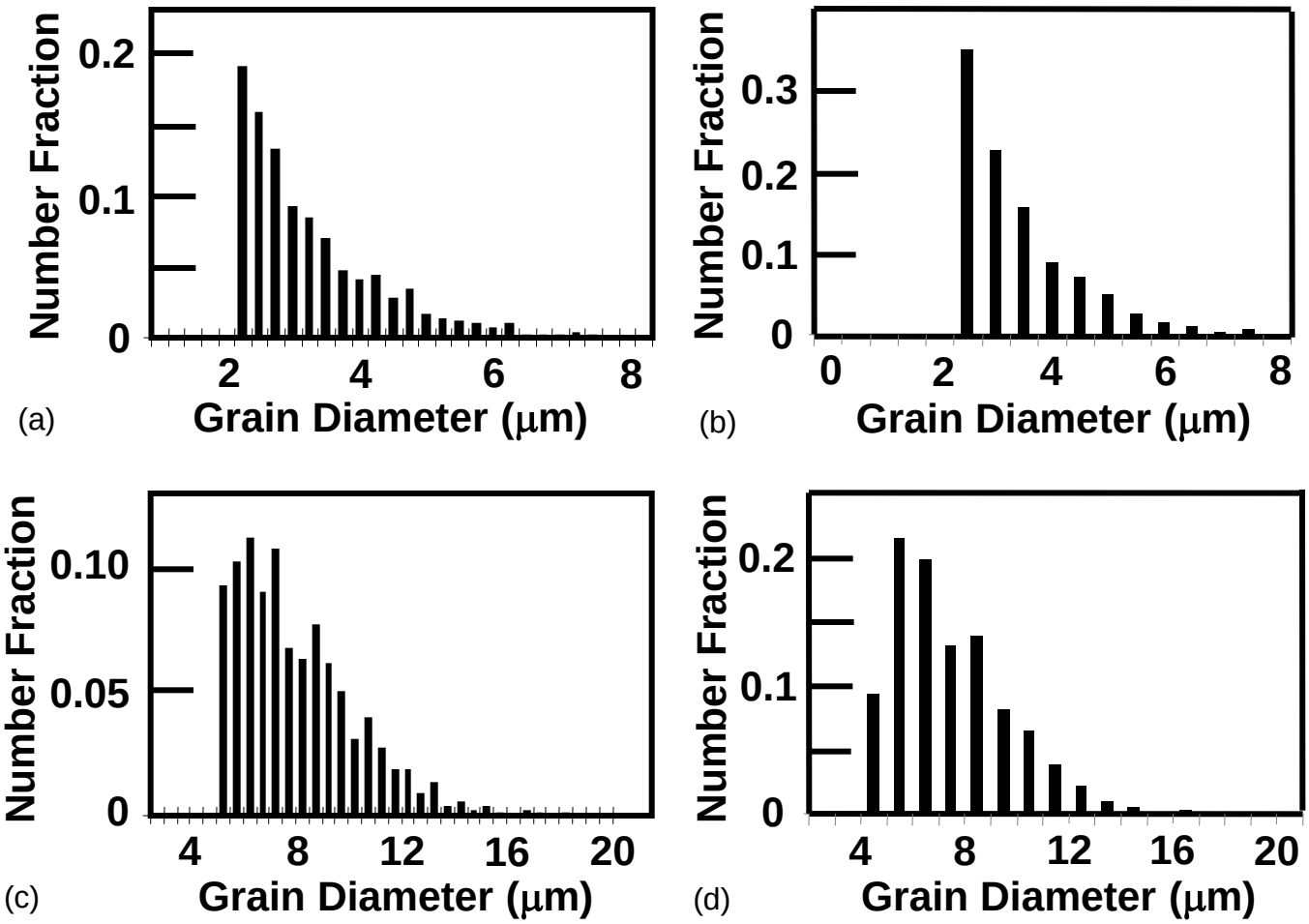

Figure 18. Approximate histograms of the gamma grain-size distribution extracted from segmented images of 230-mm-diameter LSHR extrusion OD samples which were preheated 10 minutes and compressed to a 2:1 reduction at 0.0005 s^{-1} and a temperature of (a, b) 1339 K (1066°C) or (c, d) 1408 K (1135°C).